

1 **Development of Grid Corrections to Mixing Parameterizations with**
2 **Potential Application to Arctic Climate Change**

3
4 Richard T. McNider,^a Arastoo Pour-Bazar,^a

5 ^a*Earth Systems Science Center, University of Alabama in Huntsville, Huntsville, Alabama*

6
7 *Corresponding author:* Richard T. McNider, mcnider@nsstc.uah.edu

8
9
10 Submitted to Journal of Applied Meteorology and Climate

13

ABSTRACT

The response of the Earth's climate system to GHG forcing appears largest in the Arctic, both in observations and models. However, in multi-model evaluations (CMIP3 through CMIP6), most models appear to underestimate the amount of warming. Here, we examine the role of turbulent parameterizations of the stable boundary layer (SBL) in impacting the magnitude of warming and the spread in model responses. Turbulent parameterization of the SBL has long been a challenge in models. Forms used in high-resolution research boundary layer models often do not work well in coarser grid operational or climate models. GCM vertical resolution often deteriorates to a few layers in the SBL and 500m or more in deeper stable layers (SL). This resolution may not capture well the correct strength/depth of the Arctic inversion, the entrainment warming as the SBL is destabilized by GHG forcing, or the correct energy budgets. It seems likely that the large spread in GCM Arctic simulations is in part due to the differences and misapplications of these grid-dependent parametrizations. In this investigation, we plan a new approach to the SBL parameterization problem by explicitly incorporating grid vertical resolution in the parameterization. This will be carried out by analytically and numerically recovering a stability correction function that depends on the grid spacing. Initial tests of an analytically recovered correction function indicate that the correction function provides longer-tailed stability functions for coarse grid models. Applying this correction to a simplified Arctic profile made coarser grid models agree better with fine-scale results.

33

34

SIGNIFICANCE STATEMENT

This article addresses how small-scale turbulence may impact large-scale climate change response in coarse grid climate models. The impact of climate change in models is dependent on the vertical grid resolution in models. The present investigation proposes and tests a model correction which makes model results less grid dependent. It may help bring climate model and small-scale boundary layer communities together.

40

41

42

43

44 **1. Introduction**

45 Here, we provide background on Arctic warming and how it is related to turbulence
46 parameterizations, which are problematic in coarse vertical grid climate models. A prime
47 tenet of climate change theory is that warming in the Arctic will be much larger than over the
48 rest of the globe – this is referred to as Arctic Amplification (AA). However, in Global
49 Climate Model (GCM) evaluations (CMIP3 through CMIP6), most models appear to
50 underestimate the amount of warming (Swanson 2013, Davy and Outten, 2020, Hahn et al.
51 2021) compared to observations. We focus on the possible roles turbulent mixing in the
52 stable boundary layer (SBL) and deeper stable layers (SL) might have in climate simulations.

53 Turbulent parameterizations in gridded models for stable layers have historically been
54 known to depend on model resolution (e.g., Zilitinkevich and Esau, 2003; Savijarvi, 2009;
55 Beljaars et al., 2012) Here, we provide a preliminary analysis of a path to make stable
56 boundary layer (SBL) and deeper stable layer (SL) modeling less dependent on grid spacing.
57 This will be carried out by analytically defining a stability correction function that depends
58 on the grid spacing. It has particular importance for climate models trying to capture warming
59 rates in the Arctic because of GCMs' coarse resolution. The new correction function is tested
60 in idealized Arctic environments (GABLS1- see Cuxart et al., 2006). The GABLS1 tests
61 show that the model solution without correction is dependent on grid resolution. The larger
62 grids depart more from the baseline 2m grid. However, the simulations with the correction
63 show that the larger grids come closer to the 2m grid solution.

64 In the summary, we suggest that further understanding, refinements, and testing of our
65 approach are needed to reduce grid dependence in model performance. In the simple
66 GABLS1 setting, the model top was 400m, so the largest grid was only 60m. Testing should
67 be done in more realistic deep Arctic domains where climate model grids can be 100m to
68 500m.

69

70 **2. Background on Arctic Amplification and Role of Boundary Layer
71 Processes**

72 Arctic Amplification (AA) has been considered a signature of greenhouse gas warming,
73 as articulated by Manabe and Wetherald (1975) and Bindoff et al. (2013). In early studies
74 (Manabe and Stouffer, 1994; Hall, 2004), the primary process for enhanced high-latitude

75 warming was snow/ice albedo feedback. In a warming world, snow/ice cover would be
76 reduced, decreasing surface albedo and leading to further warming.

77 However, as discussed by Graversen and Wang (2009), polar amplification can occur
78 without changes in surface albedo. Other processes may also contribute to polar amplification
79 (Taylor et al., 2013; Pithan and Mauritsen, 2014), including confining long-wave heating to a
80 smaller depth because of the polar inversion. Sea ice loss can change not only the albedo but
81 also surface fluxes and heat budgets (Boe et al., 2009; Bintanja et al., 2012). Finally, high
82 latitude warming is affected by meridional heat transport. Part of the development of deep
83 stable layers is due to the advection of warm air aloft as part of the polar direct cell. Cai and
84 Lu 2007 noted that the enhanced poleward heat transport aloft under climate change enhances
85 the Arctic inversion, amplifying high-latitude warming. AA is exceedingly complex (Boeke
86 et al. 2021) and models often have to deal with it not from first principles but from complex
87 parameterizations.

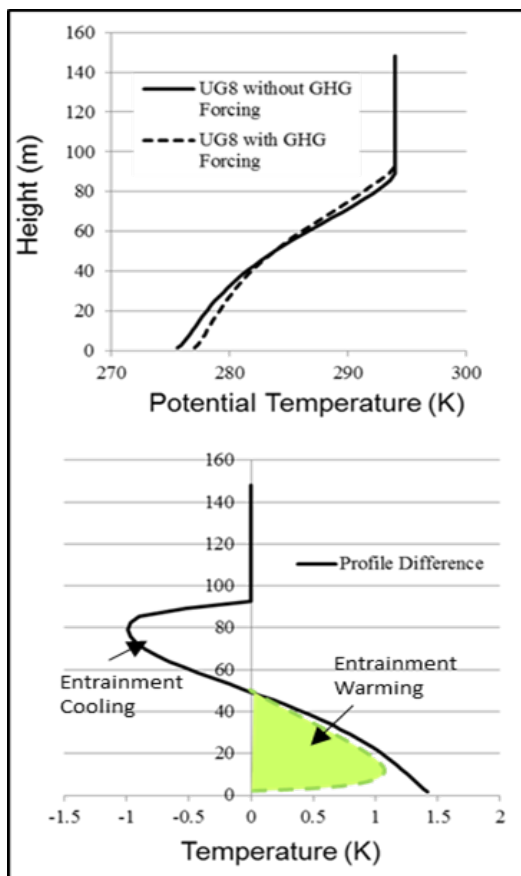
88 *a. Positive Feedback from Inversion Entrainment*

89 Studies have included the Arctic inversion as a mechanism for surface warming and AA
90 (Boe et al., 2009). For example, Davy and Esau (2014) and Bintanja et al. (2012) discussed
91 that the strong Arctic inversion confined CO₂ downward LW to a shallow surface layer,
92 thereby amplifying its impact. However, there does not seem to have been explicit
93 consideration of the role turbulent entrainment has in amplifying surface warming beyond
94 simply confining the warming to a shallow layer. Figure 1 from McNider et al. 2012
95 (hereafter MCN12, a mid-latitude study) shows an examination of a stable profile subjected
96 to enhanced greenhouse gas forcing of approximately 4 W m⁻². The top figure shows that the
97 forcing has destabilized the inversion. The lower figure shows that the destabilization
98 increases the surface temperature but cools the layers aloft. As shown in MCN12 most of the
99 warming seen at the surface was due to the entrainment of heat from aloft (the cooling at the
100 top of the profile in 1b.) In fact, MCN12 showed nearly 10 times more heat in the near-
101 surface atmosphere is due to this entrainment than the accumulation of direct greenhouse gas
102 energy.

103 In the Arctic, this would warm the ocean/melt ice. Models with sufficient vertical
104 resolution should capture this entrainment process, and part of the surface warming discussed
105 in Davy and Esau (2014) and Bintanja et al. (2012) is undoubtedly partly due to entrainment.
106 Entrainment amplification depends on the strength of the inversion and resolution in the

model. As discussed by MCN12 the amount of this entrainment warming is highly dependent on the particular stable boundary layer parametrization employed. Stable boundary layer parameterizations with less mixing (stronger initial inversions) would be more sensitive to extra GHG forcing due to greater entrainment. On the other hand, GCMs that have too much mixing in the base state (before enhanced GHG forcing) would underestimate the entrainment warming and AA. This is also consistent with Bintanja et al. 2012 (see discussion below).

113



114

Fig. 1. (top) The impact on potential temperature profile between the case of added GHG energy and base case for a geostrophic wind of 8 ms^{-1} . (bottom) Expanded view of profile difference. Colored green area shows the approximate warming due to entrainment which is much larger than the direct CO₂ warming (the remaining white area). From McNider et al. 2012.

119

120 *b. Uncertainties in GCM Performance and Warming Sensitivity at High Latitudes*

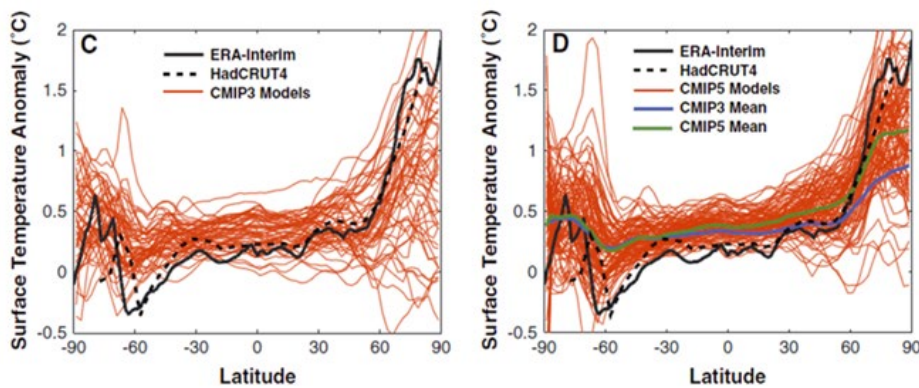
121 There have been several assessments of model inter-comparisons of AA under the CMIP3
122 through CMIP6 programs (Swanson 2013; Franzke et al. 2017; Cai, S. et al. 2021; Hahn et
123 al. 2021; Cai, Z. et al. , 2021). Figure 2 shows the comparison of CMIP3 and CMIP5 trends
124 and the comparison by Swanson (2013) to observational-based analyses – ERA-Interim and

125 HadCru4. We note that ERA-Interim is an ECMWF reanalysis product that incorporates
126 observations into a model framework. It has since been replaced by a new reanalysis – ERA5
127 - which has been available since 2018. However, Hahn et al. 2021 used ERA-Interim
128 apparently because of a slightly smaller bias for ERA-Interim in the Arctic than its successor,
129 ERA5. The Swanson (figure 2) and Hahn et al. latitudinal plots show that model spread is
130 largest at high latitudes in both hemispheres, with the spread being greatest in the Arctic.
131 Their analyses show that the mean warming in the CMIP3 and CMIP6 models is larger than
132 observations (ERA Interim, HADCRUT4, HaDCRUT5). Yet, the CMIP5 and CMIP6 greater
133 warming in high latitude, perhaps, comes at the expense of overwarming at lower latitudes.
134 Hahn et al. 2021 noted that if warming in the CMIP6 models is normalized by the global-
135 mean value, the CMIP5 and CMIP6 yield a similar degree of AA. CMIP3 and CMIP5 models
136 may simulate excessively surface-trapped Arctic warming as a result of overestimating mean-
137 state inversion strength (Pithan et al., 2014; Screen et al., 2012).

138 A recent paper by Douville 2023 discusses the continued over-prediction in the Arctic
139 from CMIP3 through CMIP6. He notes the underlying mechanisms, their seasonality, and the
140 quantification of their relative contributions to AA have been the subject of ongoing debate.
141 Further, a better understanding has not translated into much more reliable projections from
142 one generation of CMIP models to the next.

143 However, there is some recent information that may alter the view that models continue
144 to under-estimate polar warming. Tian et al. 2024, seems to cast doubt on ERA5 and ERA-
145 Interim warming in the Arctic. It is based on using a new infrared (IR) polar orbiting satellite
146 data set created by Nielsen-Englyst et al. 2023. The satellite data set shows much less
147 warming in the Arctic than ERA. We could not find any references to a response by ECMW
148 to this finding. Since the paper is new, caution is perhaps warranted at this point. We would
149 point out, based on our modeling experience, that translating surface IR temperatures to 2m
150 air temperatures depends on turbulent theory. Likewise, for ERA, extrapolating free
151 atmosphere values to 2m air temperatures depends on turbulent theory.

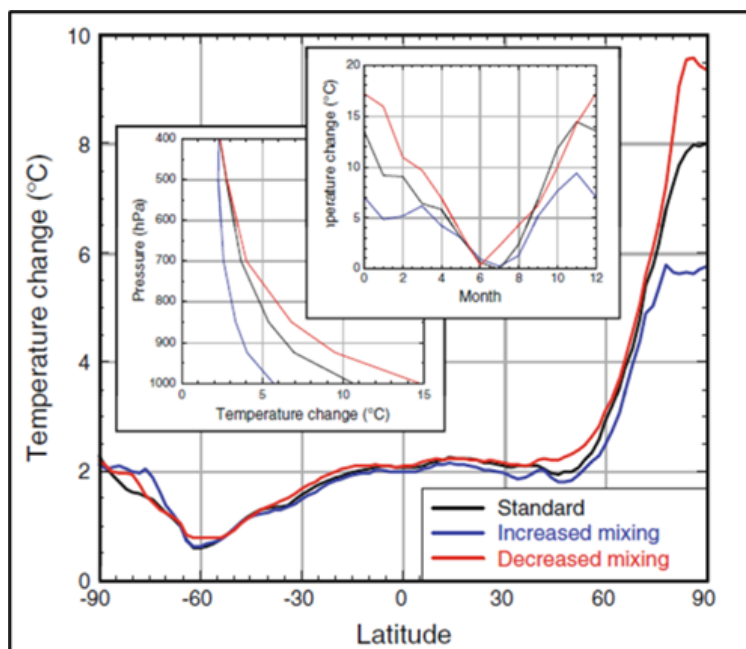
152



153

154 Fig. 2. (Adapted from Swanson 2013) Panel C shows the surface air temperature anomalies as a
 155 function of latitude for the CMIP3 simulations (red curves), as well as the ERA-Interim reanalysis (heavy
 156 black curve). The anomalies in his paper are the change in near-surface air temperatures for the 2002–2011
 157 decade relative to the 1979–2001 mean. Panel D is the same, but for CMIP5. Note ERA Interim and
 158 HadCRUT4 are observational data sets.

159 Bintanja et al. (2012) showed that in climate models, the strength of the inversion was
 160 dependent on mixing. They carried out a controlled experiment, changing mixing in a single
 161 model. Figure 3 from Bintanja et al. (2012) shows that in a GCM, the AA is tied to the
 162 amount of turbulent mixing in the high-latitude SBL. Less mixing produces a larger
 163 amplitude response in the AA. As shown in Figure 3, they demonstrate how differences due
 164 to uncertainty in SBL can impact AA in climate models.



165

166 Fig. 3. Zonal and annual mean surface air temperature change for three mixing cases (doubled CO₂).
 167 Inserts show the vertical profile of annual mean temperature change (averaged over 70–90°N), the
 168 seasonal variation of surface air temperature change (averaged over 70–90°N), and the seasonal variation
 169 of surface air temperature change (averaged over 70–90°N). (Source Bintanja et al. 2012).

170

171 *c. Modeling Difficulties for SBL Regimes*

172 The spread in model results in the Arctic may partially be due to modeling difficulties in
173 stable layers. In the 1980s, models began using local mixing schemes (e.g., Blackadar 1979;
174 Mellor and Yamada 1982) for the stable boundary layer and employing turbulent kinetic
175 energy models or stability function closures based on fundamental Monin-Obukhov
176 Similarity Theory (MOST) (Businger 1973). As a result, models began to have a problem of
177 becoming too stable, with surface conditions becoming too cold and calm (Derbyshire 1999).
178 Mixing of heat and momentum to the surface was too weak (Louis 1979; Beljaars and
179 Holtslag 1991; Viterbo et al. 1999; Beljaars et al. 2012; Audouin et al. 2021). In these coarse
180 grid operational models, it appeared that additional mixing was needed (Savijarvi 2009;
181 Viterbo et al. 1999). Thus, mixing formulations that had more mixing were employed, such
182 as longer-tailed stability functions – see below. Bintanja et al. (2012) also discussed the bias
183 in the ECMWF IFS model and referenced the adjustments made by Viterbo et al. (1999) to
184 add mixing for operational forecast purposes. They noted that such adjustments may not be
185 appropriate in climate models, in that too much mixing can impact the sensitivity of the
186 climate model to GHG forcing.

187 In K closure models in the stable layer, such as those used in GCMs and weather forecast
188 models (Esau and Byrkjedal 2007), the vertical mixing coefficient is often parameterized
189 (Blackadar 1979; McNider et al. 1981; Savijarvi 2009) by

190
$$K_m = f_m(Ri)l^2s \quad K_h = f_h(Ri)l^2s \quad f_m = Pr(Ri) f_h \quad (1)$$

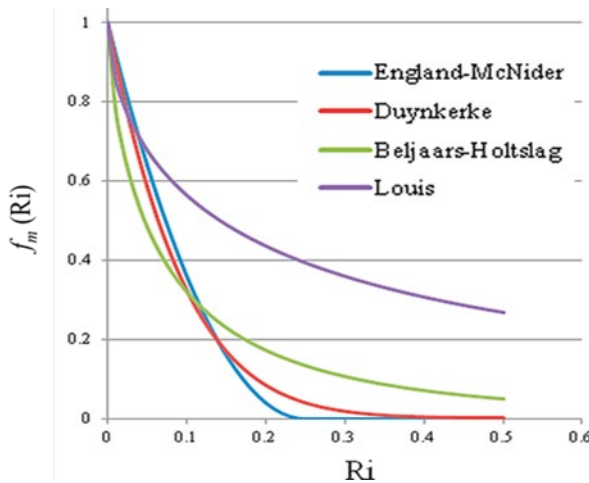
191 Here K_m , K_h are the mixing coefficients for momentum and heat. The symbols $f_m(Ri)$,
192 $f_h(Ri)$ are referred to as the stability functions with Ri , the Richardson Number, given by

193
$$Ri = \left(\frac{g}{\theta_0}\right) \left(\frac{\partial \theta}{\partial z}\right) / \left(\frac{\partial V}{\partial z}\right)^2.$$

194 The symbol l is a mixing length, s is the local shear, and Pr is the Prandtl Number. Here, we
195 will refer to $f_h(Ri)$ generically as $f_s(Ri)$, then $f_m(Ri)$ can be recovered using the Prandtl
196 Number (see Pleim 2007). Esau and Byrkjedal (2007) provide an excellent overview of the first-
197 order closure/recovery of $f_m(Ri)$ and $f_h(Ri)$ from LES databases. Note that this stability
198 function closure is basically a TKE model with the advection of turbulence ignored.

199 Originally, Blackadar (1979) and others based the stability function on boundary layer
200 observations in which turbulence was suppressed beyond an $Ri \sim 0.25$. Fig. 4 shows the typical
201 stability functions used in the SBL in the past. The England-McNider and Duynkerke would be

short-tailed forms, more consistent with Monin-Obukov Similarity Theory (MOST) (MCN12) and LES results, while the Beljaars-Holtslag and Louis forms would be considered longer-tailed forms having enhanced mixing at larger Ri . As discussed by Savijarvi (2009), the added mixing needed by operational models was often implemented by using the longer-tailed stability functions (Beljaars and Holtslag 1991; Viterbo et al. 1999).



207

Fig. 4. Typical stability functions used in modeling the SBL. Ri is the gradient Richardson number. See England and McNider (1995), Duynkerke (1991), Beljaars and Holtslag (1991) and Louis 1979). The Duynkerke, Beljaars and Holtslag, and Louis represent curve fits to the original parameterization. See also Van de Wiel et al. 2002a.

212

213 Early on, as local turbulent closures were being implemented, investigators (e.g.,
214 Blackadar 1979; Shir and Bornstein 1977; McNider and Pielke 1981) argued for the need for
215 additional mixing in coarse grid models beyond the cutoff at a critical Richardson Number
216 (Ric) of ~ 0.25 . The physical argument was based on the existence of unresolved fine-scale
217 shear and temperature gradients in the real atmosphere that contributed to mixing. It was also
218 felt that horizontal heterogeneity might also contribute to mixing (Mahrt 1996; Steeneveld et
219 al 2008b). However, as shown below, perhaps part of the reason is how the discretized form
220 of Ri is defined, which is explicitly dependent on grid spacing and not just missing
221 unresolved structure. This is the focus of the present investigation.

222 Besides the longer-tailed stability functions, other mixing adjustments, such as making
223 Ric an ad hoc function of grid spacing (McNider and Pielke 1981) or setting minimum
224 diffusivities (Pleim 2007), were employed to add mixing and to keep the model from being
225 too cold. We note also that Galperin et al. (2007a) also discussed that Ric is not a fundamental
226 measure of when turbulence is suppressed due in part due to other forms of mixing.

227 Today, however, it appears that with increased vertical resolution and/or improved
228 radiation schemes, some operational forecast models are now making the opposite error with
229 these adjustments, having too much mixing (Steenneveld et al 2008a; Savijarvi 2009;
230 MCN12). The spread in temperature in the GABLS1 single column model intercomparison
231 (Beare et al. 2006) and GCM Arctic Amplification (Swanson 2013; Hahn et al. 2021) is likely
232 in part a result of historical variations in the issue of parameterizing mixing in SBL.

233 *d. Other Modeling Frameworks*

234 The present work on a grid-corrected stability function has used the diffusion coefficient
235 (K , stability function) approach in (1). Some models may have more complex TKE
236 formulations for local mixing in the stable layers (Mellor and Yamada 1982; Kantha and
237 Clayson 1994; Basu et al. 1999) that may be a more robust modeling approach. But they have
238 similar issues with vertical resolution and with the stability function forms. One well-known
239 TKE closure is the MYJ formulation (Janjic, 2001) based on Mellor (1973) and Mellor and
240 Yamada (1982). The MYJ form has been used in the 3-dimensional operational forecast
241 models. Another framework is the Quasi-Normal Scale Elimination (QNSE) (Sukoriansky et
242 al., 2005); Sukoriansky 2008), which solves for turbulent energy in Fourier space. Galperin et
243 al. 2007b showed that the QNSE system, with coarser resolution than LES, performed as well
244 or better than LES. However, even the TKE schemes and QNSE have to parameterize the
245 sub-grid or small wavelength mixing (Tastula et al., 2015a). They use

246
$$K = \alpha l S \sqrt{TKE}$$

247 Where α is a non-dimensional coefficient, S is the inverse of a stability function, l is a
248 turbulence length scale, and TKE is the turbulence kinetic energy. As discussed by Tastula et
249 al. (2015a), one of the differences between MYJ and QNSE is the form of the stability
250 function. The MYJ has a shorter-tail form with K 's shutting off at small Ri , while the QNSE
251 form has a longer-tail with K 's being maintained well beyond an Ri of 1. Thus, these
252 complex schemes may also need adjustment for grid spacing. Recently, Casasanta et al.
253 (2025) provided an extensive review of Monin-Obukov Similarity Theory (MOST) and how
254 it can be derived from a new closure - Energy and Flux Budget (EFB). Importantly, it shows
255 that the specific similarity forms can be derived without empirical fitting.

256 Higher-order turbulence physical space closures and QNSE involve more complex
257 mathematical equations and calculations than simpler schemes. This increases the
258 computational cost and processing time, which can be problematic for the long-duration runs

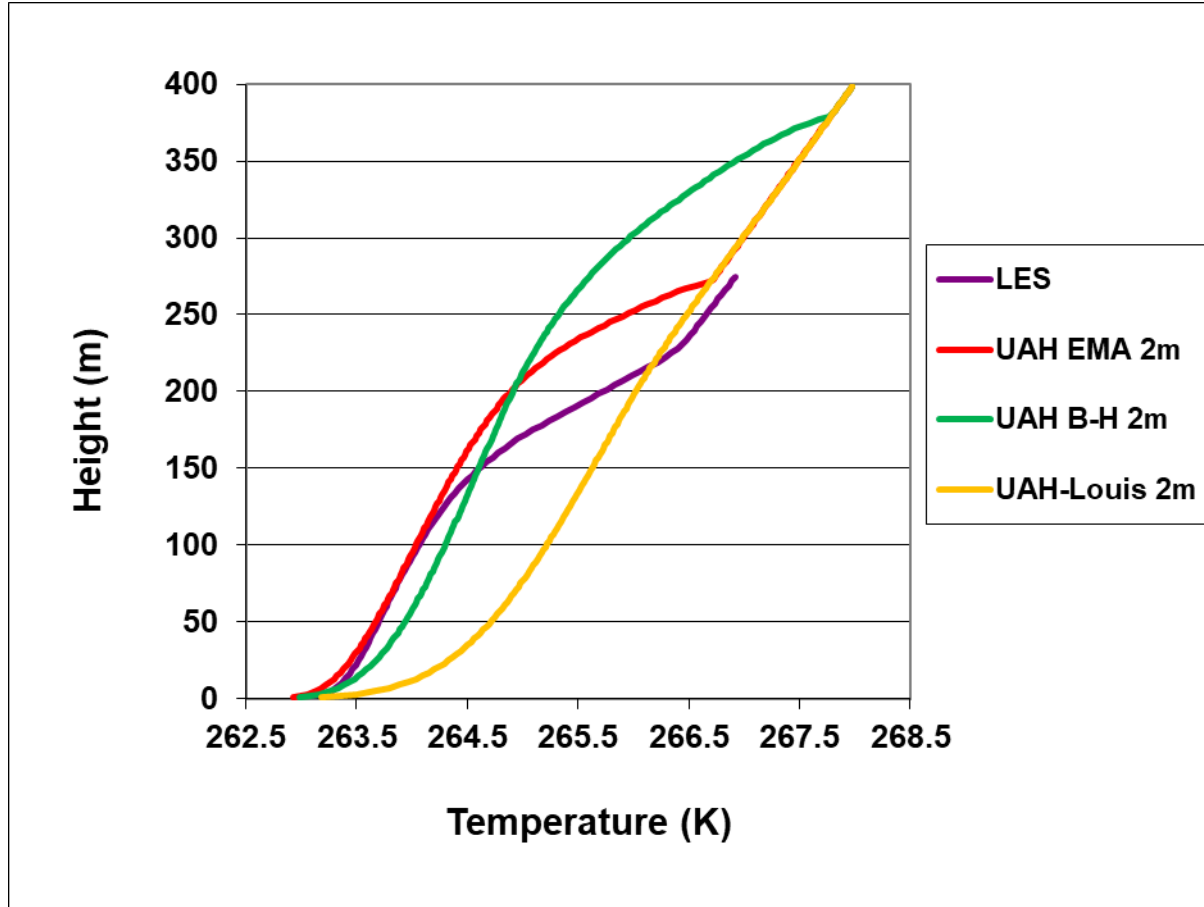
259 required for 3-D global climate models (GCMs). We are not fully familiar with the
260 computational costs of QNSE. It has been used to good effect in a 1-D model (WRF)
261 simulation in the Sichuan Basin (Wang et al. 2024). We note that recently it was used as one
262 of the PBL schemes in a study of winds in 3-D high-resolution simulations on Tibetan
263 Plateau (Dong et al. 2025).

264

265 *e. Impact of Mixing Parameterizations on Arctic Profiles and Energy Budgets*

266 Different SBL parameterizations can greatly impact profiles of temperature. Figure 5
267 shows the development of an idealized Arctic stable boundary layer for several different
268 mixing parameterizations using a single-column model for a GABLS1 boundary layer test
269 case. It employs the UAH single-column model – see McNider et al. 2012 for a description.
270 See Cuxart et al. (2006) and below for a description of the test case.

271



272

273 Fig. 5. Comparison of the different stability functions run in the UAH model against the GABLS1
 274 single column model Arctic inter-comparison case [see Cuxart et al., 2006]. The LES came from the LES
 275 ensemble reported by Cuxart et al. [2006]. The UAH EMA is simulation with the exponential stability
 276 function used in the present study. The B-H and Louis curves are runs with the UAH model using the
 277 Beljaars-Holtslag stability function and the Louis function. Note also that these longer-tailed forms were
 278 employed in the high-resolution UAH model, not in the coarser grids for which they were developed.

279

280 In Figure 5, the UAH-EMA form is the exponential approximation (see below) of the
 281 original England-McNider (England and McNider 1995) form in Figure 4. The EMA form is
 282 close to the Duynkerke form. The shorter-tailed UAH-EMA form is more consistent with
 283 the LES simulations, which have even less mixing. The Beljaars-Holtslag (B-H) and Louis
 284 stability functions were developed to add mixing needed in coarse-resolution weather
 285 forecasting and climate models. The performance of these longer-tailed profiles in their
 286 original coarse resolution setting would be different than the UAH model with high vertical
 287 resolution (2m). But this does show the sensitivity of the SBL to parameterizations and the
 288 important role of model vertical resolution. We also note that the MYJ and ONSE also do
 289 very well compared to LES in the GABLS1 setting (Tastula et al., 2015b).

290

291 *f. Importance of Correct Transition Between Strongly and Weakly Stable States*

292 Recent studies of the SBL have shown the importance of correctly capturing the
293 transition between weak and strong stability states as a function of external parameters (Van
294 de Wiel et al 2012; Van de Wiel et al. 2017; Acevedo et al 2021). This is because the
295 transition between the two states has a large impact on average SAT, surface heat flux, and
296 temperature profiles. Vignon et al (2017) concluded that correctly capturing the transition
297 was critical to establishing and maintaining the pervasive inversion in the Antarctic. They
298 further showed that this transition was both a function of turbulent parametrizations and
299 model vertical grid resolution.

300 Vignon et al. (2017) also used several stability functions. They employed a long-tail form
301 between the Louis and Beljaars, and the Holtslag form seen in Figure 4. This form is referred
302 to as L82 in their paper. They also employed two shorter-tail forms, the first one similar to
303 the Duynkerke form in Figure 4. They also used the England and McNider form. They
304 showed that higher resolution simulations and short-tailed stability functions agreed best with
305 the observations. But, in coarse grids, the short-tail forms did not produce enough mixing.

306

307 **3. Role of Model Vertical Resolution to Improve Understanding of
308 Modeled AA**

309 As discussed above, the SBL is sensitively dependent on model vertical resolution. Under
310 the present project, we will attempt to develop improved SBL parameterizations within the
311 context of equation (1) by creating a correction to the short-tailed stability function $f_s(Ri)$
312 dependent on model vertical resolution. More recently, Esau and Byrkjedal (2007) provided
313 an excellent review of the resolution issue, providing several examples of the sensitivity error
314 to model vertical resolution. Byrkjedal et al. (2008) showed GCM performance in the Arctic
315 deteriorated with coarser resolution. Thus, resolution is a critical issue in global climate
316 modeling, in that the coarse vertical resolution in GCMs may not capture the correct
317 strength/depth of the Arctic inversion, the entrainment warming discussed above, or the
318 correct energy budgets (MCN12). In particular, Vignon et al. (2017) showed that while the
319 shorter-tailed (EM) form performs best in higher resolution models, they couldn't

320 recommend these for GCM resolutions since they produced runaway cooling because of too
321 little mixing over the Antarctic Plateau.

322 *a. Development of Grid-Dependent Correction Function*

323 The improvement of parameterization within the context of (1) will be carried out by
324 developing a grid resolution correction to the stability function $f_s(Ri)$. As noted above, the most
325 fundamental theoretical forms for the stability functions in the stable boundary layer are the
326 short-tailed forms in Fig. 4 (such as England and McNider and Duynkerke), which are derived
327 from the Monin-Obukhov Similarity Theory - MOST (Businger 1973). But at larger vertical grid
328 spacing, they don't produce enough mixing. The correction function we analytically derive
329 produces a longer-tailed function for larger grids, which adds mixing.

330 We believe that examining the discretized form of (1), which is how it is used in numerical
331 models, may be a somewhat fresh approach to this long-running SBL issue. For analytical
332 simplicity, all the stability function forms in Fig. 4 can be well approximated by an exponential
333 function

334
$$f_s(Ri) = e^{-\frac{\gamma Ri}{Ric}}, \quad (2)$$

335 where large γ yields a shorter-tailed form. A value of $\gamma=3.2$ approximates the shorter tail
336 England McNider form seen in Figure 4 and was used in the present study. Ideally, the results of
337 parameterizations should not depend on the grid spacing. Thus, to preserve the integrity of the
338 simulation in coarse grid models, $f_s(Ri)$ may need to be a function of vertical grid spacing Δz .
339 Thus, we desire to find a correction function $f_c(Ri, \Delta z)$ such that

340
$$\frac{d}{d\Delta z} (f_s(Ri)f_c(Ri, \Delta z)) = 0 \quad (3)$$

341

342 We assume that the short-tailed form works well for a small Δz and call this small reference
343 grid spacing Δz_r . Next, use the finite difference or discretized form of Ri (mentioned by Walters
344 et al. 2007)

345
$$Ri = \left(\frac{g}{\theta_0}\right) \frac{\frac{\Delta\theta}{\Delta z}}{\left(\frac{\Delta V \Delta V}{\Delta z \Delta z}\right)} = \left(\frac{g}{\theta_0}\right) \frac{\Delta\theta}{\Delta V^2} \Delta z \quad (4)$$

346 Here, note, the dependence of Ri on Δz , with larger Δz giving a larger Ri for a given constant
347 $\frac{\Delta\theta}{\Delta V^2}$. A larger Ri would reduce the amount of mixing. As background, the observational

348 community has long used a discretized form of Ri and called it a bulk Ri number when the
 349 spacing of observations can be large. See Stull 1988. This, Stull noted, then requires a larger
 350 critical Ri to maintain mixing. Fernando and Weil 2010 also have shown a near-linear increase in
 351 Ri as the vertical spacing in measurements increases (their Fig. 2). This is consistent with the
 352 extensive discussion above of the need for more mixing in models at larger Δz . However, there is
 353 a caveat. If $\frac{\Delta\theta}{\Delta V^2}$ is an inverse linear function of Δz (i.e. $\frac{\Delta\theta}{\Delta V^2} = a / \Delta z$), then this behavior goes away
 354 (the implications of this are discussed below).

355 Using (4) in (3), we obtain the ODE as an initial value problem as Δz departs from Δz_r .
 356 The initial condition is $f_c(\Delta z - \Delta z_r) = f_c(0) = 1$ (i.e., no correction).

$$357 \frac{d}{d(\Delta z - \Delta z_r)} \left(e^{-\frac{\gamma(g/\theta_0)\Delta\theta}{Ric}\Delta z} f_c(Ri, \Delta z - \Delta z_r) \right) = 0 \quad (5)$$

358 It is instructive to examine the form of the ODE. If $\frac{\Delta\theta}{\Delta V^2} = a / \Delta z$, then the Δz cancels out in the
 359 first expression, implying there is no dependence on Δz . In this case, the expression is a constant
 360 and the ODE is identically zero and thus is ill-posed. This result is, perhaps, intuitive since if the
 361 gradients are linear, then the discretization would be perfect and there would be no need for a
 362 correction. This is perhaps where curvature in $\frac{\Delta\theta}{\Delta V^2}$ comes into play (suggested by Beljaars 2020),
 363 which will be discussed later.

364 We can solve this ordinary differential equation (*ODE*) analytically with a specific
 365 assumption about the functional dependence of $\frac{\Delta\theta}{\Delta V^2}$ on Δz . Assume that $\frac{\Delta\theta}{\Delta V^2}$ is a constant. Then
 366 the *ODE* (5) can be solved analytically to find f_c . Let $v = \Delta z - \Delta z_r$, $dv = d\Delta z$, $\Delta z = v + \Delta z_r$,
 367 then

$$368 \frac{d}{dv} \left(e^{-\frac{-\gamma(g/\theta_0)\Delta\theta}{Ric}(v + \Delta z_r)} f_c(Ri, v) \right) = 0.$$

369 By expanding the derivative and separating, we arrive at

$$370 \frac{df_c}{f_c} = \left(\frac{\gamma}{Ric} \right) \left(\frac{g}{\theta_0} \right) \frac{\Delta\theta}{\Delta V^2} dv.$$

371 Next, integrating with $\frac{\Delta\theta}{\Delta V^2}$ a constant, the solution is

$$372 \ln f_c = \left(\frac{\gamma}{Ric} \right) \left(\frac{g}{\theta_0} \right) \frac{\Delta\theta}{\Delta V^2} v + C.$$

373 Using the initial condition from above, $f_c(0) = 1$, then C=0. So that

374
$$f_c(\Delta z - \Delta z_R) = e^{\left(\frac{\gamma}{Ric}\right)\left(\frac{g}{\theta_0}\right)\frac{\Delta\theta}{\Delta V^2}(\Delta z - \Delta z_r)} \quad (6)$$

375

376 However, note that from (3) above $\left(\frac{g}{\theta_0}\right)\frac{\Delta\theta}{\Delta V^2}\Delta z = Ri$. Therefore, we can substitute this
377 definition in f_c to write the solution in terms of Ri

378
$$f_c(\Delta z - \Delta z_R) = e^{\left(\frac{\gamma}{Ric}\right)Ri\left(1 - \frac{\Delta z_r}{\Delta z}\right)} \quad (7)$$

379 But, with the caution that the form of this solution is based on $\frac{\Delta\theta}{\Delta V^2}$ being a constant, or
380 equivalently, Ri a constant. However, we can plot the solution for different values of this
381 constant ($\frac{\Delta\theta}{\Delta V^2}$) or Ri . Thus, while this form shows what the solution might look like for different
382 Ri , the form of the solution might be different if the variation of Ri with z had been included in
383 the solution of the ODE. Since the solution is not exact for the general case (i.e. Ri not a constant)
384 to partially account for this uncertainty, we add a variable (D) representing the uncertainty in the
385 exact form of the solution. We can use D to explore the sensitivity of the correction function

386
$$f_c(\Delta z - \Delta z_r) = e^{D\left(\frac{\gamma}{Ric}\right)Ri\left(1 - \frac{\Delta z_r}{\Delta z}\right)} \quad (8)$$

387 Since $f_c(\Delta z)$ is a correction function applied to $f_s(Ri)$, we now look at the product

388
$$f_s * f_c = e^{-\frac{\gamma}{Ric}Ri} * e^{D\left(\frac{\gamma}{Ric}\right)Ri\left(1 - \frac{\Delta z_r}{\Delta z}\right)} \quad (9)$$

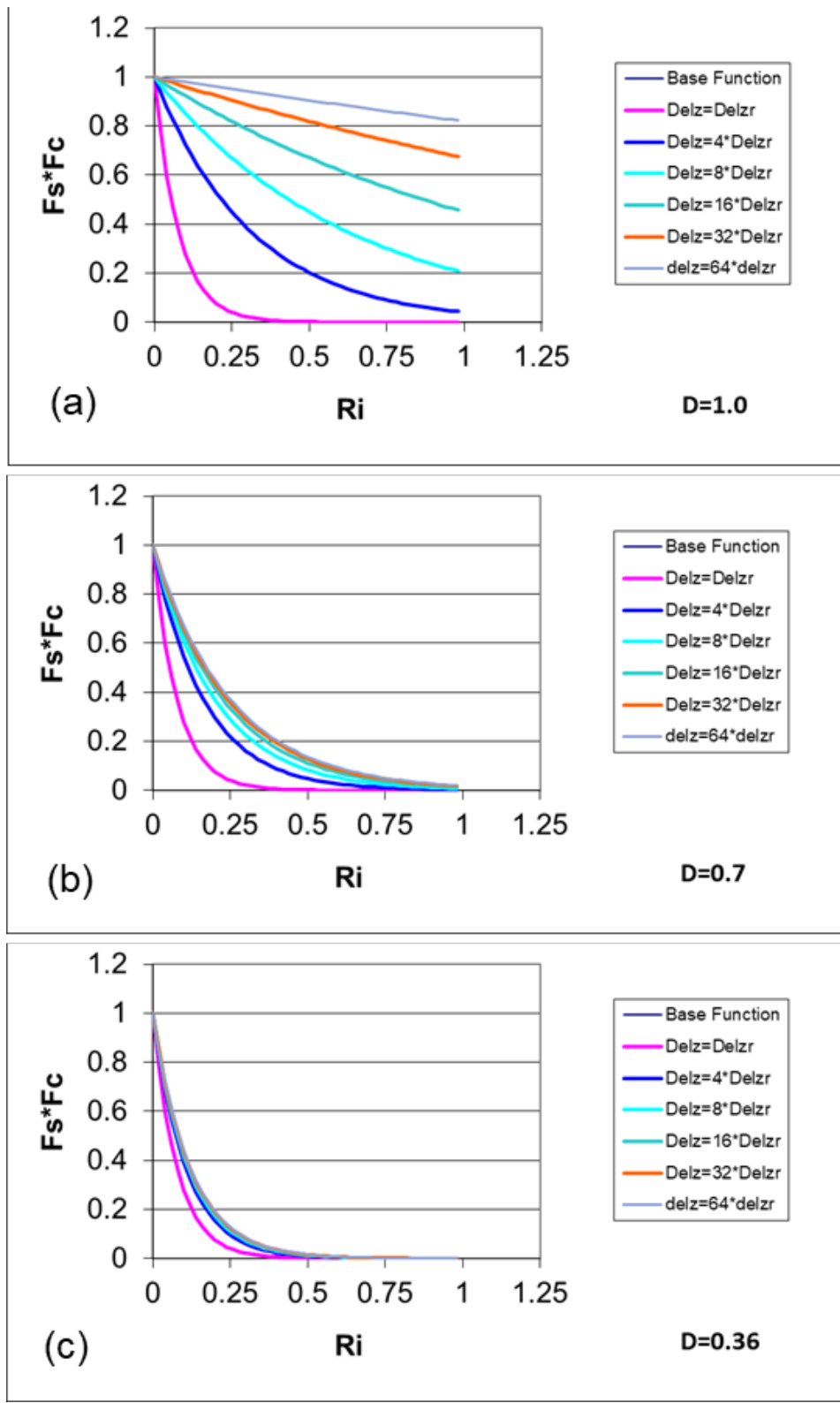
389 This can be further simplified to a form

390
$$f_{is} = f_s * f_c = e^{-\frac{\gamma}{Ric}Ri \left[\frac{(1-D)\Delta z + D\Delta z_r}{\Delta z} \right]} \quad (10)$$

391 which conveys the role of D as giving a weighted average of the exponential function by Δz
392 and Δz_r , normalized by Δz (where $\Delta z \geq \Delta z_r$). For D=0, the fraction is 1 (no correction to the
393 short-tail stability function), and for D=1, the exponent is adjusted by $\frac{\Delta z_r}{\Delta z}$, yielding a long-
394 tailed stability function for larger grid spacing. Thus, this form represents a weighted
395 combination of short- and long-tail functions, with D controlling the relative contribution of
396 each.

397 Figure 6 shows the behavior of $f_s * f_c$ for three different values of D. While the assumption of
398 $\frac{\Delta\theta}{\Delta V^2}$ being a constant is a simplification and not likely to occur in general, it is interesting that the

399 form of the analytical recovery reflects the need for longer-tailed forms at larger grid spacing. D
400 controls the amplitude of the corrected function ($f_s * f_c$) and the length of the tail. Larger D's give
401 longer tails. The ability to have longer-tailed stability function is consistent with added mixing
402 discussed by Savijarvi (2009) and Beljaars and Holtslag (1991), such as the Beljaars-Holtslag and
403 Louis forms in figure 4 that have been used in some operational and coarse grid models.



404

405 Fig. 6. Behavior of the correction function (actually $f_s^*f_c$) from (8) as a function of Ri for different
 406 values of D . Note that for a smaller Δz the correction yields a short tail form, and for a larger Δz yields a longer
 407 tail form with greater mixing. Note that the base function is covered by the $delZr$ case.

408

409

410 *b. Preliminary Tests of the Analytically Derived Correction Function*

411 In order to test the correction function in (8), we carry out a series of numerical
412 simulations for the Arctic using the UAH single column model (see Figure 5) discussed in
413 McN12. Note that the UAH model uses an explicit diffusion scheme to avoid numerical
414 diffusion (see MCN12) rather than a semi-implicit scheme used in many operational models.
415 We employ the GABLS1 single-column model inter-comparison framework (see Cuxart et
416 al., 2006), which is based on an idealized Arctic stable boundary layer (Kosovic and Curry,
417 2000). The initial components of the wind are set equal to those of the geostrophic wind
418 ($U = U_g$, $V = V_g$). The potential temperature (θ) equals 265 K up to 100 m, then it increases at a
419 rate of 0.01 K/m until the domain top (400 m), where a value of 268K is reached. The surface
420 temperature is set to 265 K initially, decreasing at a constant rate of 0.25 K/h. The value of
421 the aerodynamic roughness length (z_0) is set to 0.1 m. Note, this is a very idealized case.
422 Actual Arctic boundary layers may have fine-scale features with more complex and deeper
423 stable atmospheric structure.

424 In making the runs, we desire to have the surface momentum flux (u_*^2) and heat flux
425 ($u_*\theta_*$) consistent with the stability functions used in the atmospheric simulations (Tastula
426 2015b). Following England and McNider 1995 we define

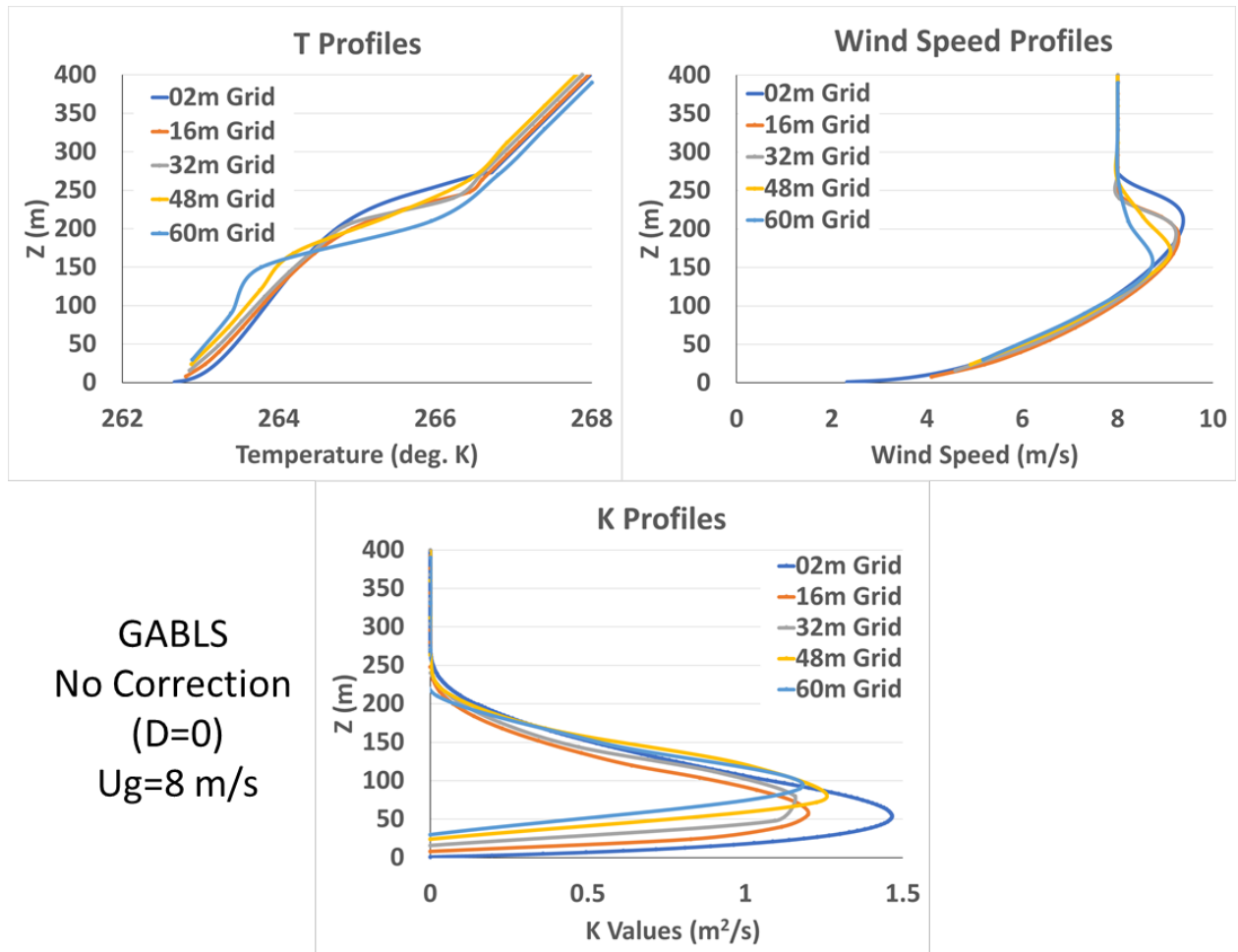
$$427 \quad u_*^2 = k^2 f_m(Ri_{1/2}) |V_1|^2 / (\ln \frac{z_1}{z_0}),$$

$$428 \quad u_*\theta_* = k^2 f_h(Ri_{1/2}) |V_1| (\theta_1 - \theta_G) / (\ln \frac{z_1}{z_0})$$

429 where k is the Von Karman constant, V_1 is the first level wind speed, z_1 is the first model
430 level, z_0 is the surface roughness, θ_1 is the potential temperature at the first level, θ_G
431 is the surface or ground temperature and $Ri_{1/2}$ is the gradient Richardson between the
432 z_0 and z_1 .

433 Here, we explore the sensitivity of the solutions to grid spacing and then examine whether
434 we can use the correction function in (8) to make the solution more independent of grid
435 vertical resolution. Figure 7 shows the model simulation of potential temperature after 10
436 hours of simulation for different grid spacings with no correction. Note that the mixing in the
437 coarser grids is less than the values for the 2 m grid. This is consistent with our original
438 formulation for Ri (see (4) above), in that Ri would be larger, indicating a reduction in $f_s(Ri)$
439 (since Ri would be shifted to the right as in Figure 4). The coarser grid also shows the

440 mixing increasing with height, but near the 250 m level, it has slightly less mixing than the
 441 finer grids. While the differences in mixing are small, the behavior of the temperature profile
 442 is quite different. Showing the sensitive non-linear behavior of the SBL (McNider et al. 1995
 443 and Van de Wiel et al. 2002a,b).

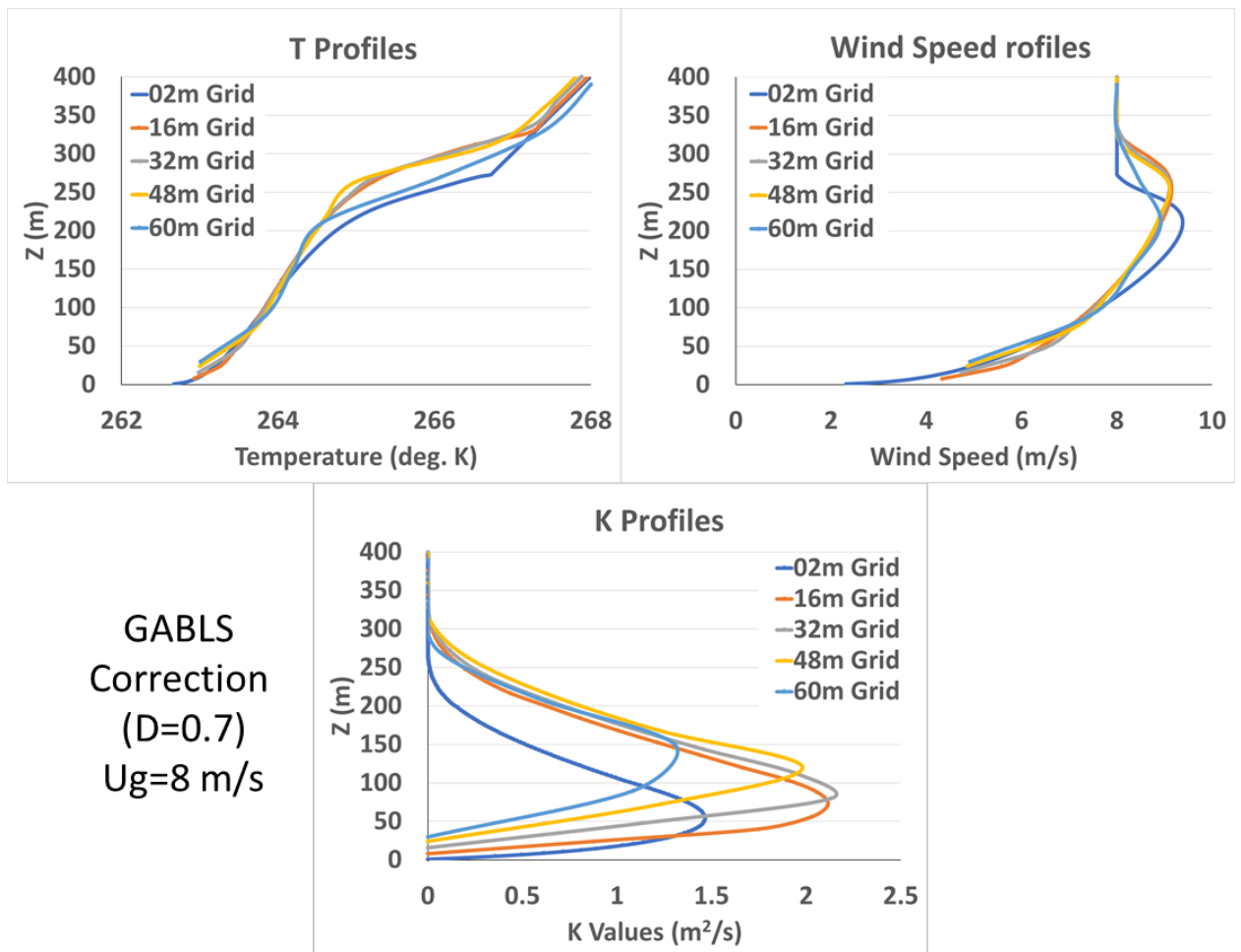


445 Figure 7 Case for No Correction. (top left) Potential temperature profile after 10 hrs of simulation for
 446 different grid spacings. (top right) wind speed profile ($m s^{-1}$) after 10 hours of simulation for different grid
 447 spacings. (bottom) average mixing values over the length of the integration for different grid spacings K
 448 ($m^2 s^{-1}$). Grid spacings are given in figures.

449
 450 Here, the differences for different grid spacing may not seem large, but in this idealized
 451 limited-height case, the largest grid was only 60 meters. In real Arctic profiles, which may go
 452 up to 10-15 km, the GCM grid spacing may be 200 - 500 m or more (Essau and Byrkjedal
 453 2007). As will be discussed later, the GABLS1 case, utilized here, is an extremely idealized
 454 barotropic case with no shear in the upper atmosphere, which would exist in real baroclinic
 455 cases. The GABLS1 framework, which is well known in the SBL community, is only used as
 456 initial proof of concept for our approach. Real cases may show much greater differences as

457 larger grid spacing and more complex profiles are used. There is also the large non-linearity
 458 in the SBL, in that small changes in mixing can lead to large changes in the SBL structure
 459 (see Mahrt 1989; Derbyshire 1999; McNider et al. 1995; Van de Wiel et al. 2002a,b).

460 We next employ the grid correction function (8). In interpreting the figures, we are
 461 looking for corrections that make the larger grid results more like the 2m or Δz_r reference
 462 grid. We first tried using $D=1$, but it produced too much mixing (similar to the Louis profile
 463 in Figure 5). Next, we tried smaller values of D . Figure 7 shows the impact of using f_c with D
 464 = 0.7. It corrects the lower part of the profile but puts too much mixing at the top of the
 465 profile. This indicates that D may need to be variable as discussed below. Note that the
 466 mixing coefficients are too large over most of the domain compared to the 2 m reference
 467 case.



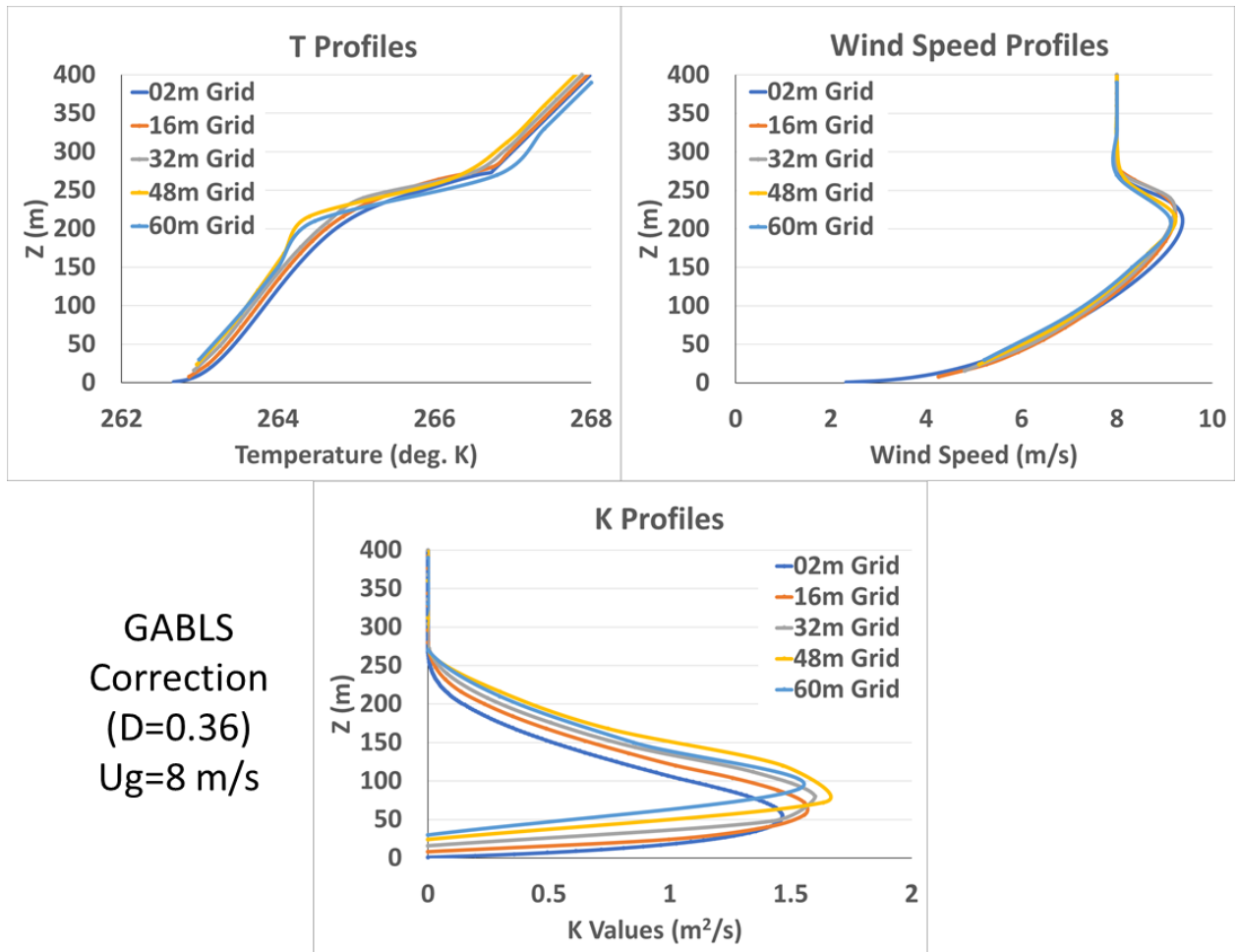
468

469 Figure 8 Case for Correction with $D = 0.7$ (top left) Potential temperature profile after 10 hrs of
 470 simulation for different grid spacing. (top right) Wind speed profile ($m s^{-1}$) after 10 hrs of simulation for
 471 different grid spacing. (bottom) Average mixing values over the length of the integration for different grid
 472 spacings K ($m^2 s^{-1}$). Grid spacings are given in figures.

473

474 Figure 9 shows the result with $D = 0.36$. It shows that the different grids can be corrected
 475 to have a solution mostly like the 2m reference case. However, the lower part of the profile
 476 correction is not as improved as the $D = 0.7$ case in Figure 11. Note also in Figure 9 (that the
 477 mixing coefficients have been corrected to be more in line with the 2m reference case.

478



479

480 Figure 9 Case for Correction with $D= 0.36$. (top left) Potential temperature profile after 10 hrs of
 481 simulation for different grid spacing. (top right) Wind speed profile (m s^{-1}) after 10 hrs of simulation for
 482 different grid spacing. (bottom) Average mixing values over the length of the integration for different grid
 483 spacings $K (\text{m}^2\text{s}^{-1})$. Grid spacings are given in figures.

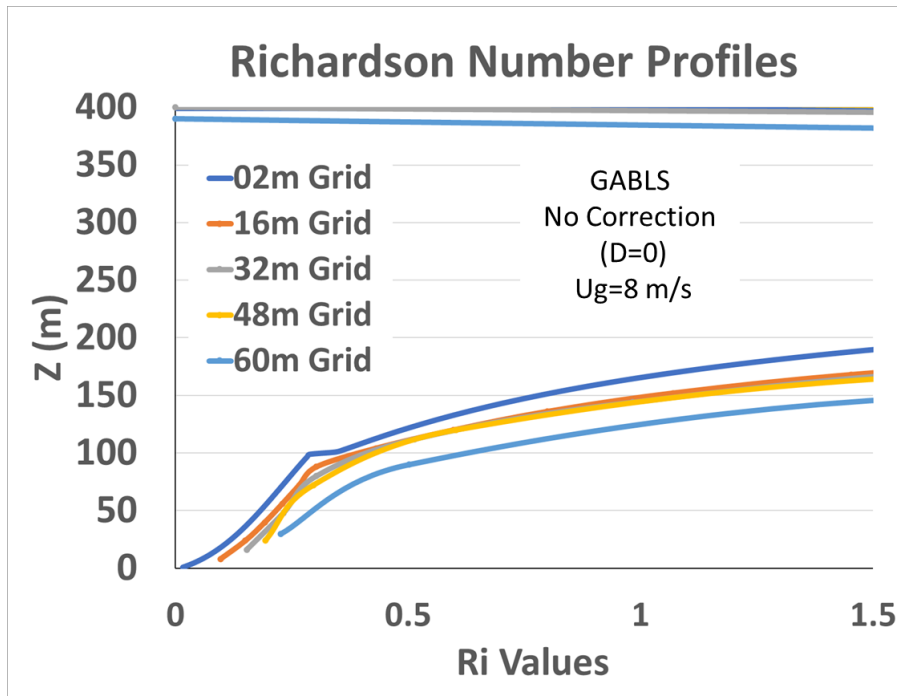
484 c. *Improved Specifications to the Parameter "D" in the Analytical Solution*

485 The analytical correction in equation (8) is appealing because of its structure and
 486 computational efficiency. It only takes two additional lines of code - one line to compute f_c
 487 (8) and one to compute the product $f_s * f_c$. The correction, which effectively yields longer-tailed
 488 stability functions for larger grids, is based on $\frac{\Delta\theta}{\Delta V^2}$ being a constant, which in effect is for R_i
 489 being constant. This is not in general true. The examples in Figures 8 and 9 show that the

490 correction functions can make model predictions less grid dependent. However, it also shows that
 491 different values of D can impact the correction. Given the fact that the ODE is ill-posed for linear
 492 gradients (i.e. no correction needed), it seems that one path might be to make D a function of the
 493 curvature in $\frac{\Delta\theta}{\Delta V^2}$ or equivalently Ri (suggested by Beljaars 2020). Here we explore D as a
 494 function of curvature in Ri, i.e. D ($d^2(Ri)/dz^2$). Under this proposed framework, D becomes
 495 smaller as gradients in Ri become linear.

496

497 Figure 10 shows a plot of Ri for the case of “No Correction” given in Figure 7. Note this is
 498 the average value of Ri over the length of the integration (10 hours), consistent with the average
 499 K values in figures 7-9. Visually, the average curvature (concave upward) is largest below about
 500 40 m, and between 40 m and 90 m, there is less curvature. Near 75 m, the curvature changes sign
 501 (concave down). Above 100 m, the curvature becomes less but remains concave downward. Note
 502 also that the curvature is smaller in the larger grids.



503

504 Figure 10 Plot of Ri for the Case of No Correction given in figure 7. These are the average values of Ri
 505 over the length of the run (ten hours). Note that curvature (concave upward) is largest below about 40 m.
 506 Between 40 m and 90 m there is less curvature. Near 75 m, the curvature changes sign (concave down). Above
 507 100 m the curvature becomes less but remains concave downward. Note also that the curvature is smaller in the
 508 larger grids. Also, note the concave up region near the ground is not well captured in the coarse grids.

509

510 Making D only a function of curvature in Ri would be the most consistent with our analytical
511 theory. But we found in tests that this provided insufficient correction near the surface. This
512 seems related to the inability for the curvature stencil to capture the correct curvature in the coarse
513 grid (see figure 12). As noted above $D=0.36$ provides a correction which makes the coarser grids
514 look more like the finer grid solution. Thus, we felt the correction needed a minimum value. In
515 adding curvature, we explored D being a linear function of curvature. We used a linear function

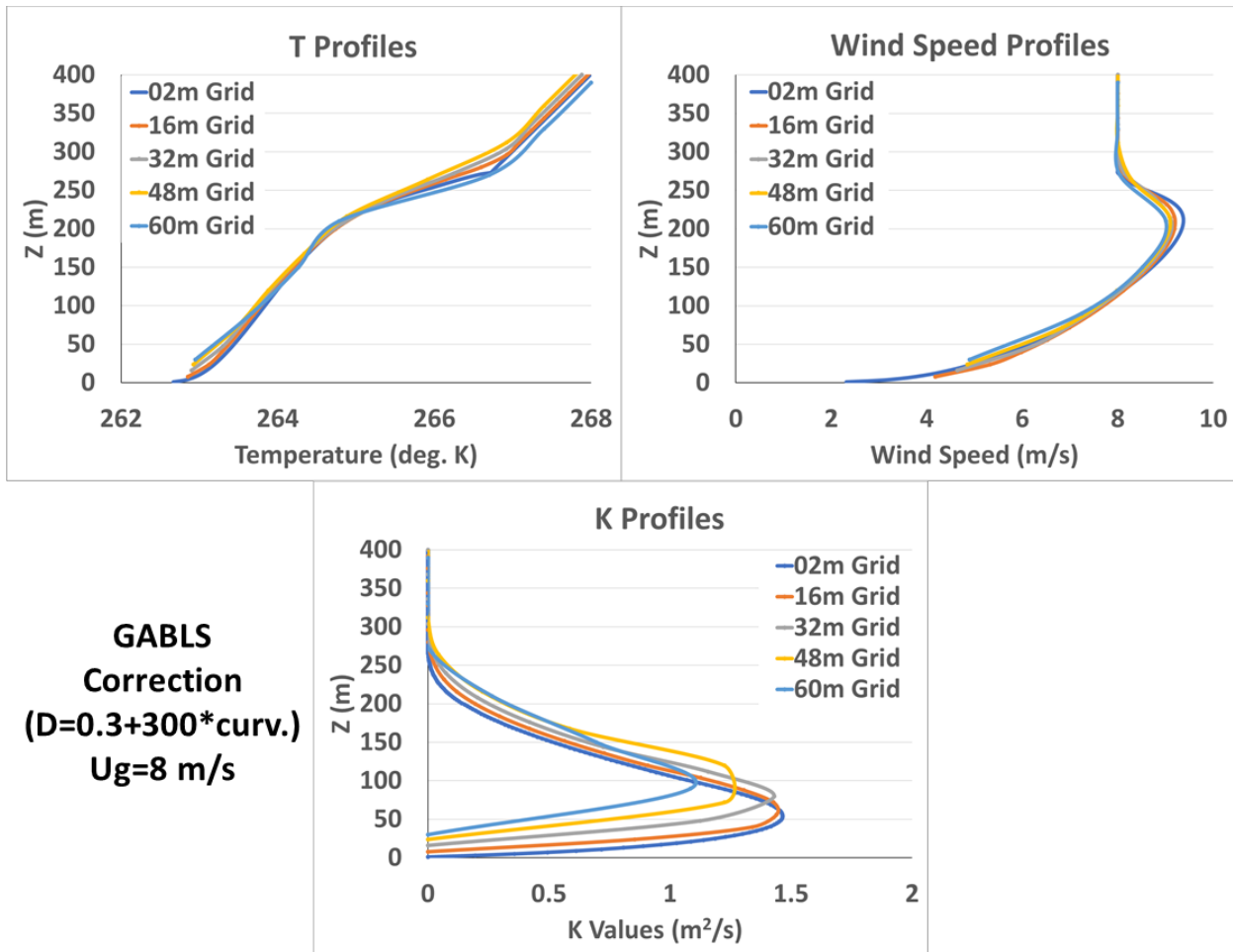
516
$$D = D_0 + M * |(d^2(Ri)/dz^2)|$$

517 where D_0 is the intercept (minimum value) and M is the slope. For curvature, $d^2(Ri)/dz^2$, we
518 employ the absolute value of the curvature since the sign of the curvature should not be relevant.
519 Since a value of $D=0.36$ as seen in Figure 9, provides an improvement, but a value of $D = 0.7$, as
520 seen in Figure 8, provides too much mixing, we tried linear functions that bracket these values.
521 Specifically, we chose through trials that $D_0 = 0.3$ and $M= 300$ so that

522
$$D = 0.3 + 300 * |(d^2(Ri)/dz^2)| \text{ with } D < 0.7 \quad (11)$$

523 provided the best results.

524 Figure 11 shows the results of this curvature-dependent correction. It shows that the
525 curvature-dependent correction for D (8), is an improvement over $D=0.36$. The curvature
526 correction improves the upper part of the temperature profile, bringing it in line with the 2m grid
527 case. Near the bottom of the profile, there seems to be a need for further correction. However, in
528 looking at the curvature, as seen in Figure 10, it can be seen that the coarser grids do not capture
529 the amount of curvature as seen in the smaller grids. In these simulations, we used similarity
530 theory (England and McNider 1995) to specify heat and momentum from the surface up to the
531 first model layer. As discussed below, a refinement in the technique in the future could utilize the
532 curvature from surface similarity in terms of Ri rather than the grid-calculated curvature
533 employed here.



534

535 Figure 11 Case for D function of curvature (8). (top left) Potential temperature profile after 10 hrs of
 536 simulation for different grid spacing. (top right) Wind speed profile (m s^{-1}) after 10 hrs of simulation for
 537 different grid spacing. (bottom) Average mixing values over the length of the integration for different grid
 538 spacings K (m^2s^{-1}). Grid spacings are given in figures.

539

540 *d. Additional Tests of the Value of D*

541 While the improvements with the curvature-dependent D above look promising in Figure
 542 11, there is concern that the values used in equation (11) may not work well in other cases

543 We have added 10 additional cases (6 wind speeds, 2 cooling rates and 2 roughness
 544 values) to test the robustness of the curvature dependent D. These are all within the
 545 framework of the GABLS1 physical domain. The reason for maintaining GABLS1 is that
 546 this framework was designed to test different boundary layer closure models and different
 547 LES models. GABLS1 was also defined around an Arctic setting. It was meant to test how
 548 different turbulence closures embedded in weather forecast models or LES simulations would
 549 change temperature and wind profiles. Thus, issues such as different models having different
 550 surface models were eliminated by having a specified surface cooling rate.

551 Since in this paper we are looking specifically at how the turbulent closure impacts the
552 temperature and wind vertical profiles at different grid spacing, the general GABLS1
553 framework should be adequate. The GABLS1 base case above was defined with a
554 geostrophic wind of 8 m/s, a surface cooling rate of 0.25 K/h and roughness length of 0.1m.
555 However, within the general framework of fixed initial conditions, there can be different
556 wind speeds, cooling rates and roughness. These are the fundamental parameters that impact
557 boundary layer structure. Here, we carry out 6 different cases where wind speeds are changed
558 from 4 m/s to 10 m/s, 2 cases where cooling rates are changed from 0.25 to 0.5 K/h and two
559 cases where roughness was increased from 0.1 m to 0.5 m. These cases cross the thresholds
560 of very stable boundary layers to weakly stable boundary layers. We believe the additional
561 wind speeds\, cooling rate and roughness cases largely encompass the parameters that impact
562 SBL behavior (see McNider et al. 1995).

563 Figure 12 shows the first of the new cases with a geostrophic wind of 4 m/s. The figure
564 shows both the uncorrected and corrected profiles. For this low wind speed case, the solution
565 goes to a very stable boundary layer with little to no mixing. There is very little variation for
566 different grid spacings, so there is not much to correct. These very stable cases have always
567 been a challenge since there is little to no turbulence generated by shear. In the real-world,
568 non-MOST phenomena, such as gravity waves, can contribute to mixing (Galperin et al.
569 2007a).

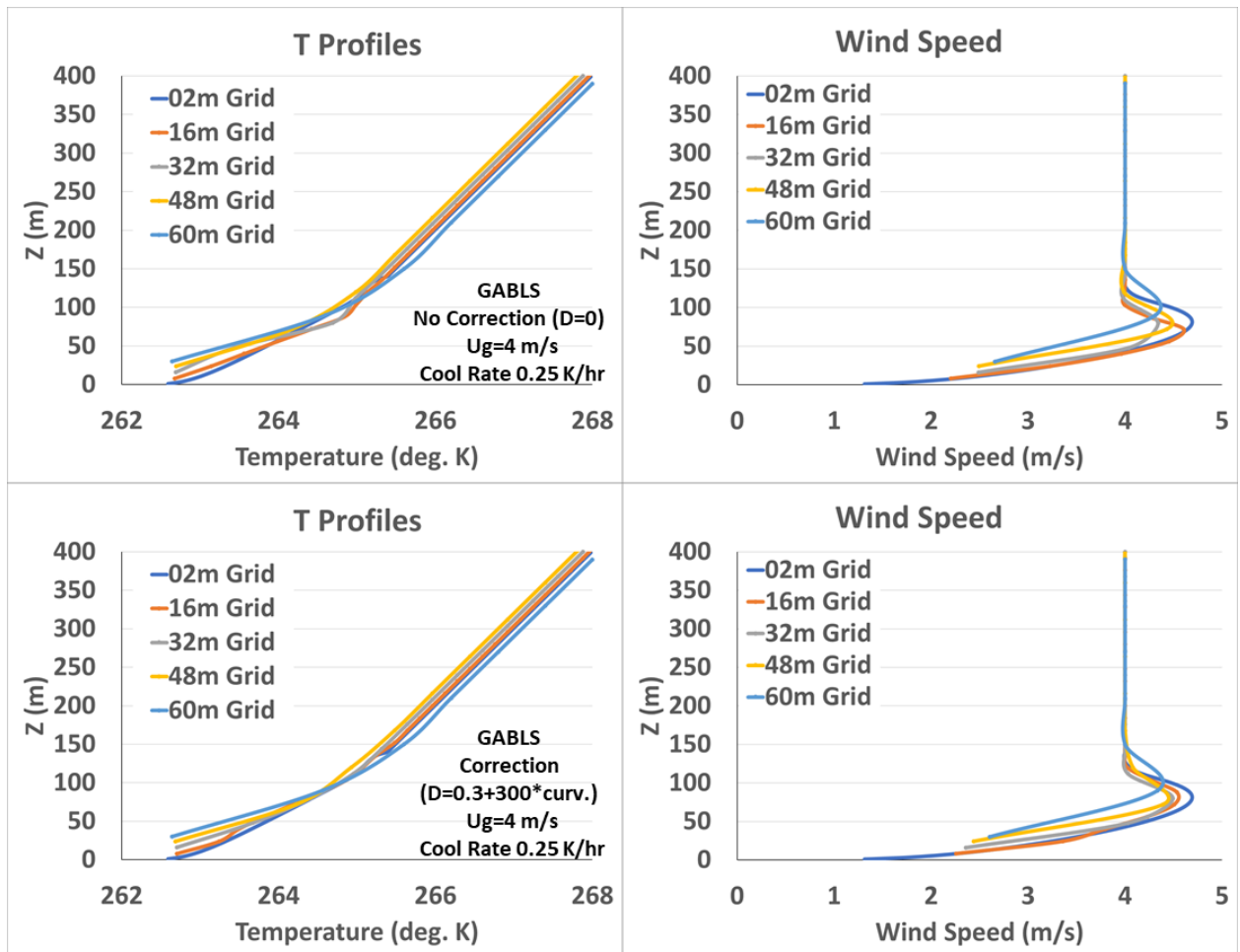
570 The following figures 13 – 20 show the other different wind speed cases. Figure 13 for 5
571 m/s geostrophic wind is similar to the 4 m/s case, but with a bit more mixing. The correction
572 does make some impact to bring the gridded solutions closer together.

573 Figure 14 shows the case for 6 m/s. Here, the SBL is transitioning from a very stable state
574 to a weakly stable state. There is a greater spread between the grid cases, and we are in the
575 regime where resolution can make a difference, as in the base GABLS1 8 m/s case given in
576 Figure 11. The correction does bring the different grid solutions closer together, especially
577 aloft.

578 Figure 15 shows the case for 7 m/s, which is close to the GABLS base 8 m/s case. The
579 correction behavior is similar to that of the base case. Figure 16 shows the 9 m/s case and
580 shows a deeper boundary layer. The correction appears to work well here, especially aloft.
581 Finally, Figure 17 shows the 10 m/s case, which yields an even deeper boundary layer. The
582 correction brings the grid cases closer together.

583

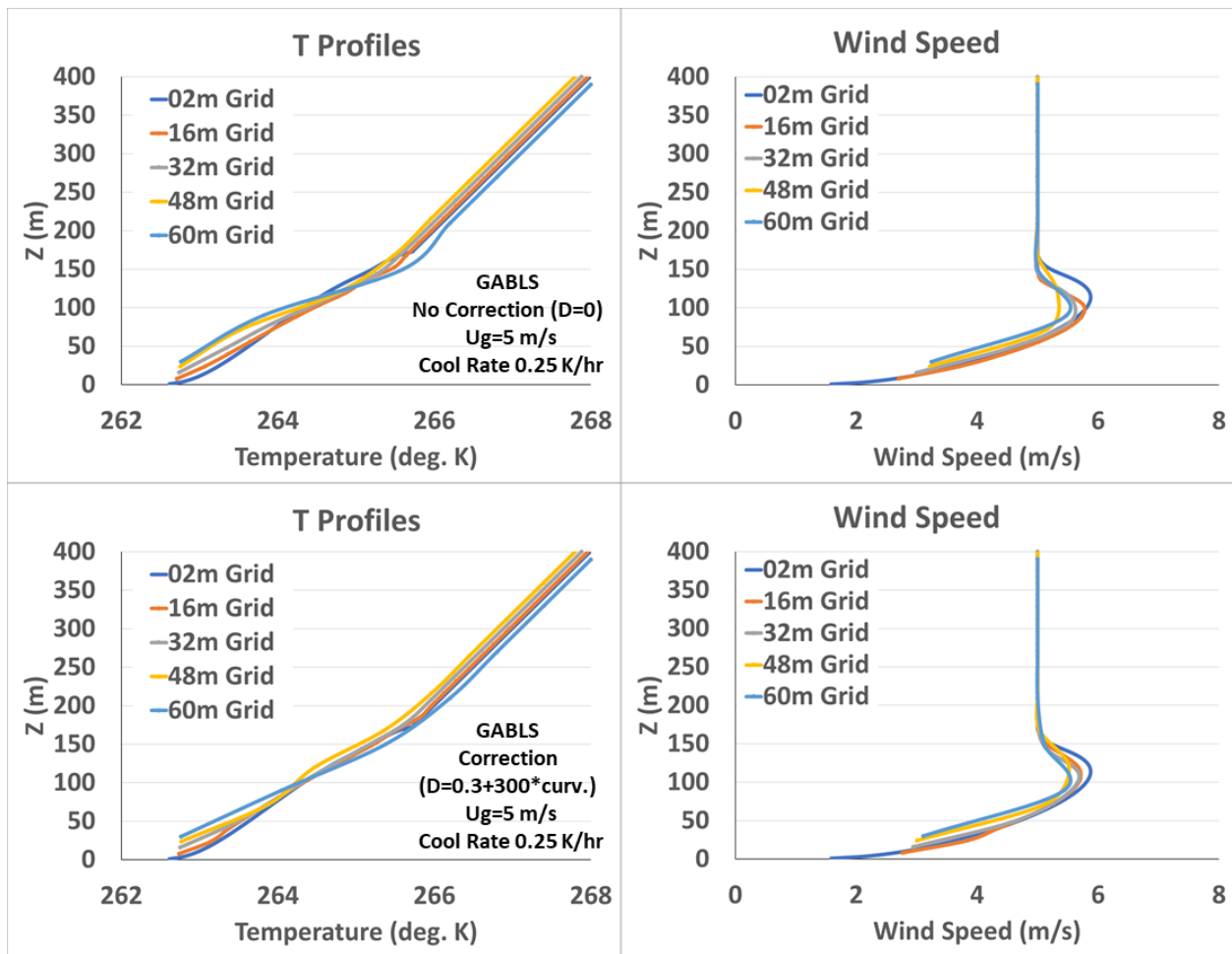
584

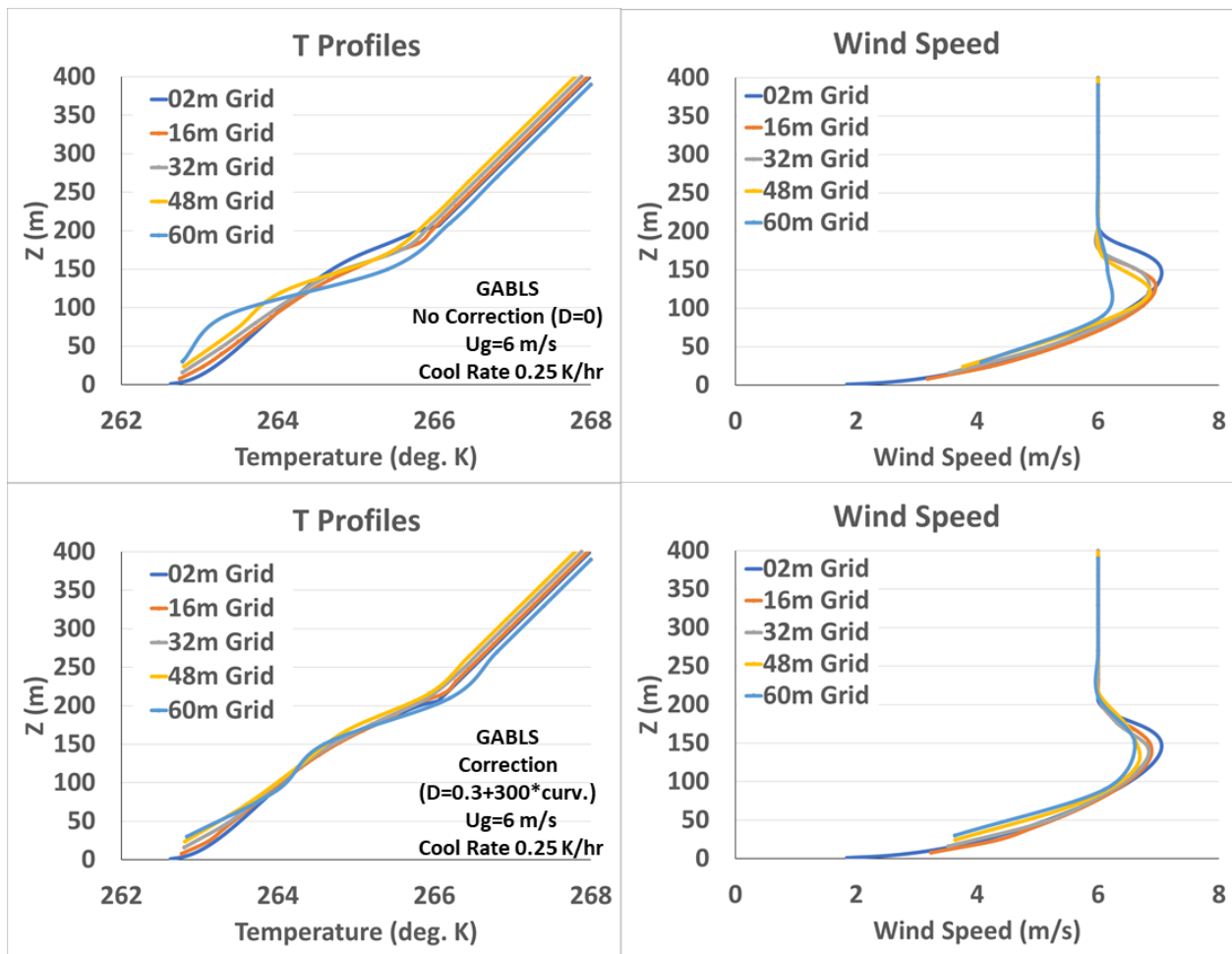


585

586 Figure 12 Plots of temperature and wind speed profiles for geostrophic wind speed of 4
587 m/s and cooling rate of 0.25 K/hr. Top uncorrected and bottom corrected using D in (8).

588





593

594 Figure 14 Plots of temperature and wind speed profiles for geostrophic wind speed of 6
 595 m/s and cooling rate of 0.25 K/hr. Top uncorrected and bottom corrected using D in (8)

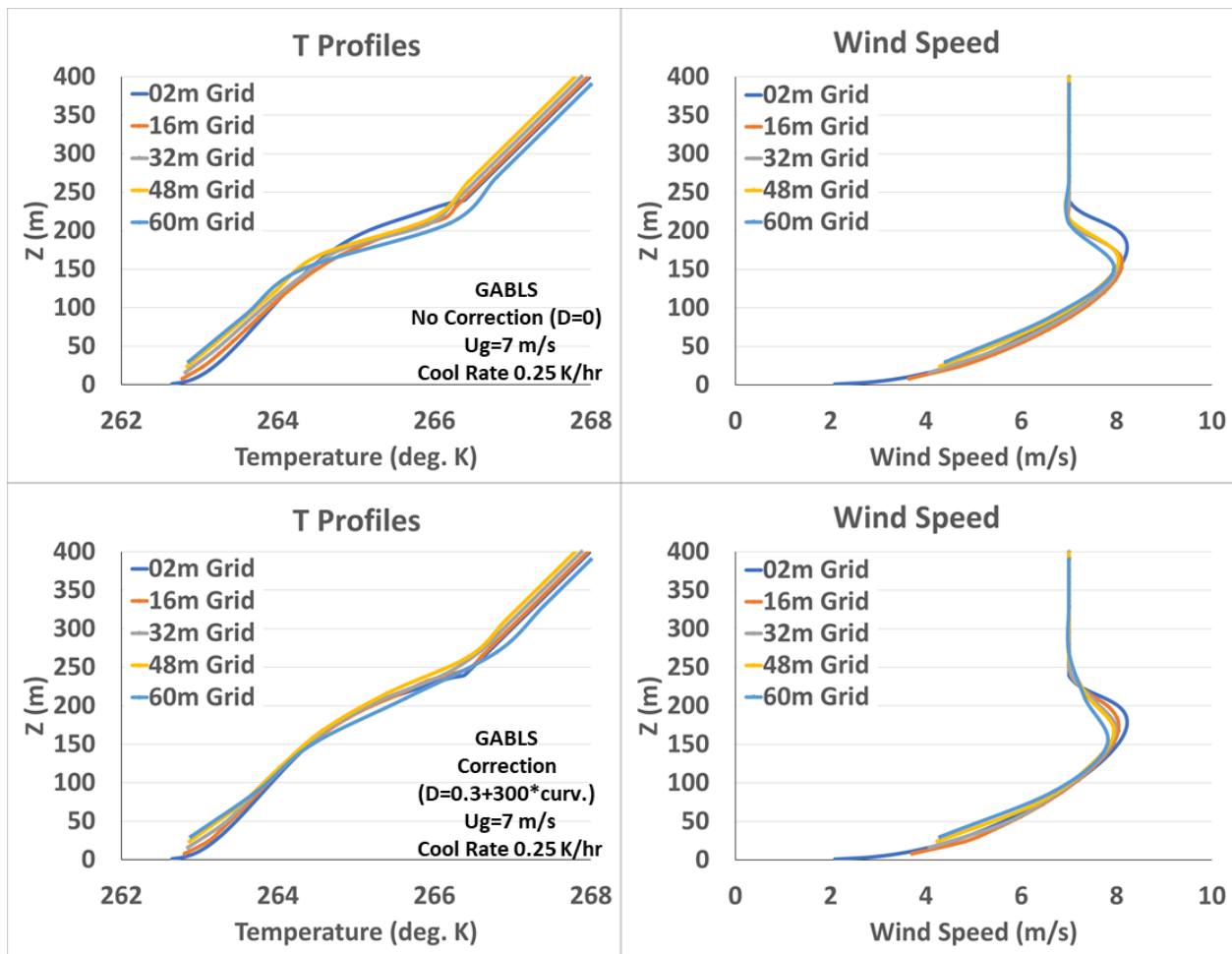
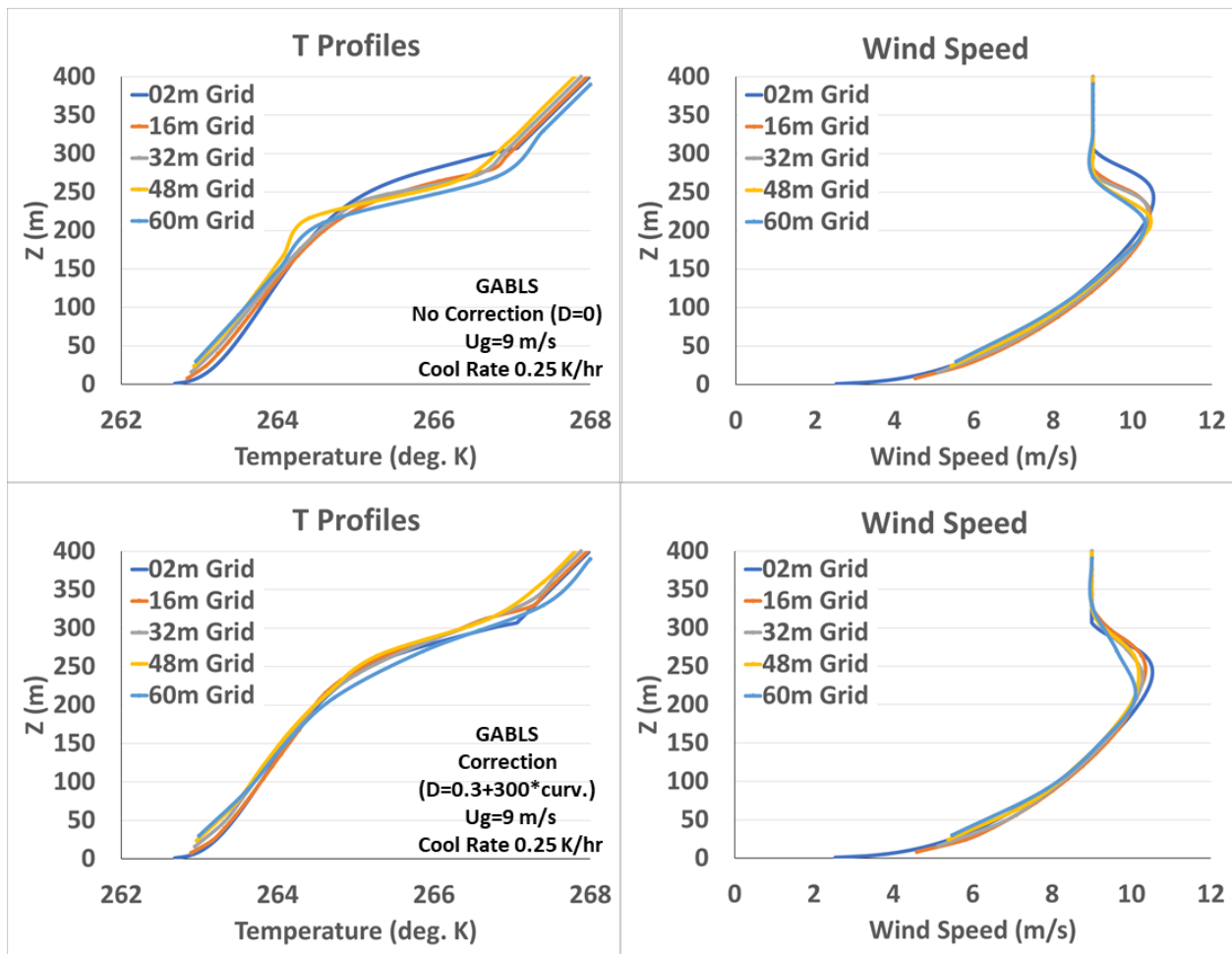
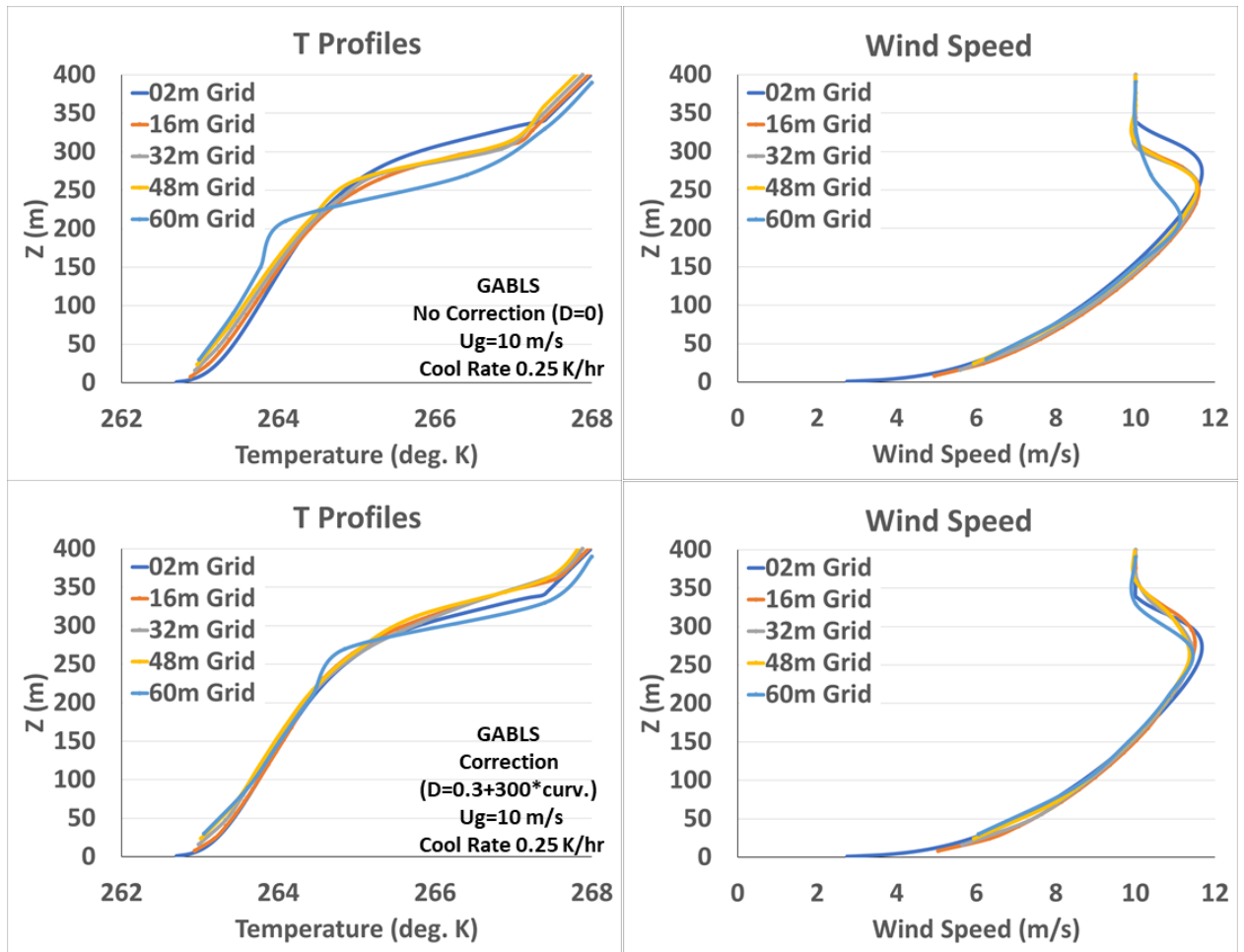


Figure 15 Plots of temperature and wind speed profiles for geostrophic wind speed of 7 m/s and cooling rate of 0.25 K/hr. Top uncorrected and bottom corrected using D in (8)



601 Figure 16 Plots of temperature and wind speed profiles for geostrophic wind speed of 9
602 m/s and cooling rate of 0.25 K/hr. Top uncorrected and bottom corrected using D in (8)
603



604

605 Figure 17 Plots of temperature and wind speed profiles for geostrophic wind speed of 10
606 m/s and cooling rate of 0.25 K/hr. Top uncorrected and bottom corrected using D in (8)

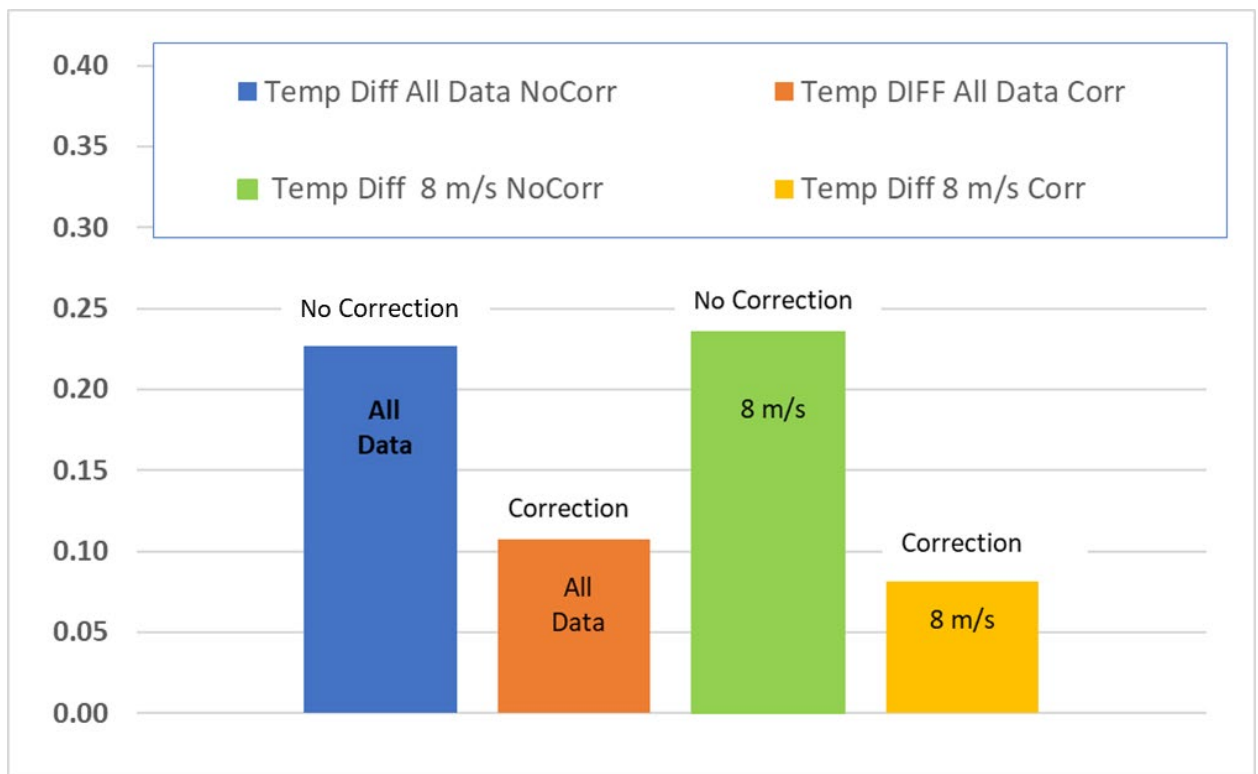
607

608 The analytical correction with the D curvature correction tested for different geostrophic
609 wind speeds appears to work nearly well as it did for the 8 m/s case, from which it was
610 derived. To quantify the impact of the corrections, we examined, for temperature and wind
611 speed, the departure of the different grid values from the 2m values (which in this case would
612 be considered the best or truth). We picked the closest 2m grid to the corresponding coarse
613 grid level. We only made comparisons for the temperature and wind speeds, which were in
614 the turbulent boundary layer. Since outside the boundary layer, the wind and temperature
615 show little to no difference from the initial specified profiles. The results are presented in
616 Figures 18 and 19. The term All Data means that the data values for all the cases in Figures
617 12-17 were compared to those of the 8 m/s case from which the D parameter was developed.
618 Some of the differences in the statistics perhaps come from the boundary layer depth
619 approximation which we used to determine where to make the difference calculations. Also,

620 the two low wind speed cases did not show as much improvement. These very stable cases
621 have always been difficult for models.

622 We also changed the cooling rates and surface roughness to evaluate the corrections. The
623 cooling rate cases were not much different in behavior and correction than the wind speed
624 cases. We increased the cooling rate from 0.25 K/ hr to 0.5 K/ hr. The results seemed
625 equivalent to lowering the wind speed in the cases above. The roughness was increased from
626 0.1 m (the GABLS1 default) to 0.5 m. The roughness cases also seemed to have a similar
627 correction. Since there was not much difference in their behavior, we include these plots in
628 Appendix B. We didn't try to quantify the correction as in figures 18-19 in part because we
629 only had two cases each. Also, the boundary depth was different than the values we
630 estimated for the different wind speeds for the GABLS1 roughness and cooling rates. We
631 used boundary layer depth to determine where to make the difference calculations.

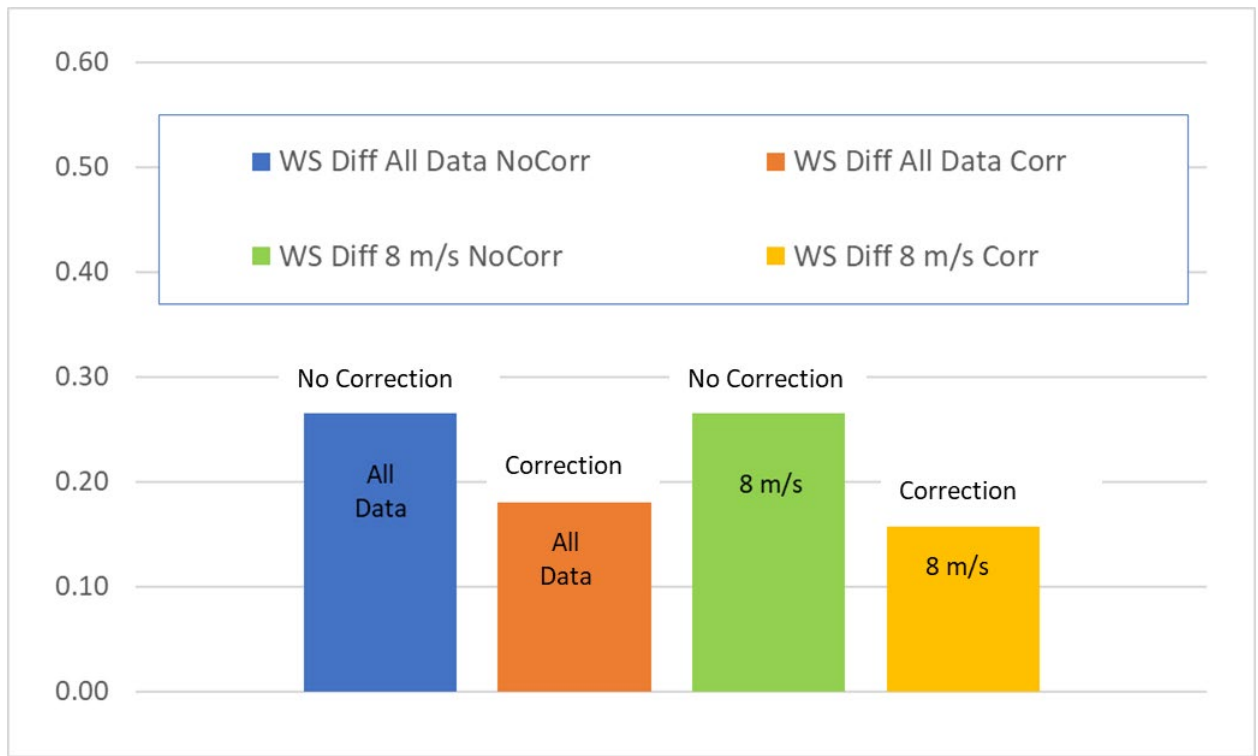
632



633

634 Figure 18 Plot showing mean differences between grid values of temperature (all levels)
635 and 2m grid (closest level) values. For All Data and the 8 m/s case.

636



637

638 Figure 19 Plot showing mean differences between grid values of wind speed (all levels)
639 and 2m grid (closest level) values. For All Data and the 8 m/s case.

640

641

642 **4 Summary and Conclusions**

643 The background on Arctic Amplification (AA) and the modeling of the SBL in coarse
644 grid climate models suggests that treatments of the SBL and deeper SL in GCMs may be
645 partly responsible for the spread seen in GCM predictions in high latitudes. This may also be
646 part of the reason models have underestimated the strength of AA. As discussed in section 2.,
647 if models have too much mixing in the base-state, they may not have the sensitivity to
648 enhanced GHG energy as models with less mixing. Also, given the difficulties with handling
649 the SBL and SL in coarse grid settings, GCMs may have other fixes that add mixing and
650 underestimate the sensitivity to GHG energy.

651 The present study provides a quantitative approach to correcting model performance in
652 predicting local turbulent levels in stable environments with different vertical grid spacings.
653 As discussed in Section 3, this has long been a problem for models using local closures, in
654 that coarser grid operational models had too little mixing. Modelers such as Louis 1979,

655 McNider and Pielke 1981, Beljaars and Holtslag 1991, and Viterbo and Beljaars 1995 added
656 additional mixing through either longer-tailed stability functions (f_s) or larger critical Richardson
657 numbers.

658 The present study provides an analytical framework for defining a correction function (f_c) for
659 the stability functions such that $\frac{d}{d\Delta z}(f_s(Ri)f_c(Ri, \Delta z)) = 0$. This ODE was solved analytically
660 under certain assumptions to recover $f_c(Ri, \Delta z)$. These correction functions were tested in a
661 simplified Arctic simulation framework GABLS1 (Cuxart et al. 2006) and found to make the
662 solutions less grid dependent.

663 A parameter D was defined which represents uncertainty because of the assumptions in the
664 analytical solution. It was found that a correction with D partially dependent on vertical curvature
665 in Ri produced solutions which were less grid dependent. A future path for investigation would
666 be to use similarity forms to estimate curvature in Ri near the surface. This may improve the
667 correction.

668 However, the assumptions that allowed the analytical solution generally are not met. A more
669 robust path may be the numerical solution of the ODE $\frac{d}{d\Delta z}(f_s(Ri)f_c(Ri, \Delta z)) = 0$. This path is
670 discussed in Appendix A.

671 In terms of Arctic Amplification, it is an extraordinarily complex system involving albedo,
672 sea ice and clouds. However, we believe it will be better to evaluate these issues in a system
673 where turbulence and grid dependence, which are also important, were handled as correctly as
674 possible. However, more work and testing are needed. Possible paths for improvements and
675 additional testing are found in Appendix A. It is hoped that this preliminary study can spur new
676 ideas and approaches by others.

677

678

679 *Acknowledgments.*

680 This work was sponsored by the Department of Energy grant #DE-SC0023332 with partial
681 support by the Alabama Office of State Climatologist. The article does not necessarily represent
682 views of DOE. We also thank the reviewers who provided positive information that improved the
683 manuscript. Particularly, we thank the reviewer who suggested additional cases to test the
684 robustness of the parameter D.

685

686 *Data Availability Statement.*

687 The model runs and code for the simulations by the UAH model (McNider et al. 2012)

688 can be found on the UAH public server

689 <https://drive.google.com/drive/folders/1rQLdJeHbTV5kjyylgo5AFXk6Ss->

690 [mQlSm?usp=sharing](#)

691

692

693 REFERENCES

694 Acevedo, O.C., Costa, F.D., Maroneze, R., Carvalho, A.D., Puhales, F.S. and Oliveira, P.E.,

695 2021: External controls on the transition between stable boundary-layer turbulence

696 regimes. *Quarterly Journal of the Royal Meteorological Society*, **147(737)**, 2335-2351,

697 <https://doi.org/10.1002/qj.4027>.

698 Audouin, O., Roehrig, R., Couvreux, F. and Williamson, D., 2021: Modeling the GABLS4

699 Strongly-Stable Boundary Layer With a GCM Turbulence Parameterization: Parametric

700 Sensitivity or Intrinsic Limits? *Journal of Advances in Modeling Earth Systems*, **13(3)**,

701 e2020MS002269, <https://doi.org/10.1029/2020MS002269>.

702 Basu, S., Raman, S., Mohanty, U.C. and Rajagopal, E.N., 1999: Influence of the planetary

703 boundary layer physics on medium-range prediction of monsoon over India. *pure and*

704 *applied geophysics*, **155**, pp.33-55, <https://doi.org/10.1007/s000240050253>.

705 Beljaars, A.C.M. and Holtslag, A.A.M., 1991: Flux parameterization over land surfaces for

706 atmospheric models. *Journal of Applied Meteorology*, **30(3)**, 327-341,

707 [https://doi.org/10.1175/1520-0450\(1991\)030<0327:FPOLSF>2.0.CO;2](https://doi.org/10.1175/1520-0450(1991)030<0327:FPOLSF>2.0.CO;2).

708 Beljaars, A.C.M. , 2020: Personal Communication.

709 Beljaars, A. C. M., and Coauthors, 2012: The stable boundary layer in the ECMWF

710 model. *Proc. ECMWF Workshop on Diurnal Cycles and the Stable Boundary*

711 *Layer*, Reading, England, ECMWF/WCRP, 1-10,

712 <https://www.ecmwf.int/sites/default/files/elibrary/2012/8029-stable-boundary-layer-ecmwf-model.pdf>

- Bindoff, N.L., Stott, P.A., AchutaRao, K.M., Allen, M.R., Gillett, N., Gutzler, D., Hansingo, K., Hegerl, G., Hu, Y., Jain, S. and Sebbari, R., 2014: Detection and attribution of climate change: from global to regional. *Climate change 2013: the physical science basis*,
- Bintanja, R., Van der Linden, E.C. and Hazeleger, W., 2012: Boundary layer stability and Arctic climate change: A feedback study using EC-Earth. *Climate dynamics*, **39(11)**, 2659-2673, <https://doi.org/10.1007/s00382-011-1272-1>.
- Blackadar, A.K., 1979: High resolution models of the planetary boundary layer. *Advances in Environmental Science and Engineering*, **1(1)**, 50-85.
- Beare, R.J., Macvean, M.K., Holtslag, A.A., Cuxart, J., Esau, I., Golaz, J.C., Jimenez, M.A., Khairoutdinov, M., Kosovic, B., Lewellen, D. and Lund, T.S., 2006. An intercomparison of large-eddy simulations of the stable boundary layer. *Boundary-Layer Meteorology*, **118(2)**, pp.247-272.
- Boe, J., Hall, A. and Qu, X., 2009: Current GCMs' unrealistic negative feedback in the Arctic. *Journal of Climate*, **22(17)**, 4682-4695, <https://doi.org/10.1175/2009JCLI2885.1>.
- Boeke, R.C., Taylor, P.C. and Sejas, S.A., 2021. On the nature of the Arctic's positive lapse-rate feedback. *Geophysical Research Letters*, **48(1)**, p.e2020GL091109.
- Businger JA, 1973: Turbulent transfer in the atmospheric surface layer. In *Workshop on Micrometeorology*, 67-100, Am. Met. Soc.
- Byrkjedal, Ø., Esau, I. and Kvamstø, N.G., 2008: Sensitivity of simulated wintertime Arctic atmosphere to vertical resolution in the ARPEGE/IFS model. *Climate dynamics*, **30(7-8)**, 687-701, <https://doi.org/10.1007/s00382-007-0316-z>.
- Cai, M., and J. H. Lu, 2007: Dynamical greenhouse-plus feedback and polar warming amplification. Part II: Meridional and vertical asymmetries of the global warming. *Climate Dyn.*, **29**, 375–391, <https://doi.org/10.1007/s00382-007-0238-9>.
- Cai, Z. et al. , 2021a: Arctic warming revealed by multiple CMIP6 models: evaluation of historical simulations and quantification of future projection uncertainties. *J. Clim.* **34**, 4871–4892.
- Cai, S., Hsu, P.-C., and Liu, F., 2021b: Changes in Polar Amplification in Response to Increasing Warming in CMIP6. *Atmos. Oceanic Sci. Lett.* **14**, 100043–102834.

- 742 doi:10.1016/j.aosl.2021.100043
- 743 Casasanta, G., Conte, M., Sozzi, R., Cecilia, A., Petenko, I. and Argentini, S., 2025. Towards
744 definitive functional forms for Monin–Obukhov similarity functions in stable and very
745 stable surface layers. *Scientific Reports*, 15(1), p.25632.
- 746 Cuxart, J., Holtslag, A. A. M., Beare, R. J., Bazile, E., Beljaars, A., Cheng, A., Conangla, L.,
747 Freedman, M. Ek, F. , Hamdi, R., Kerstein, A., Kitagawa, H., Lenderink, G., Lewellen,
748 D., Mailhot, J., Mauritsen, T., Perov, V., Schayes, G., Steeneveld, G. J. Svensson, G.,
749 Taylor, P., Weng, W., Wunsch, S. and Xu, K.-M., 2006: Single Column Model
750 Intercomparison for the Stably Stratified Atmospheric Boundary Layer, *Boundary-Layer
751 Meteorol.*, 118(2), 273-303, <https://doi.org/10.1007/s10546-005-3780-1>.
- 752 Davy, R. and Esau, I., 2014: Global climate models' bias in surface temperature trends and
753 variability. *Environmental Research Letters*, 9(11), 114024, <https://doi.org/10.1088/1748-9326/9/11/114024>.
- 754
- 755 Davy, R. and Outten, S., 2020: The Arctic surface climate in CMIP6: status and
756 developments since CMIP5. *Journal of Climate*, 33(18), 8047-8068,
757 <https://doi.org/10.1175/JCLI-D-19-0990.1>.
- 758 Derbyshire, S.H., 1999: Boundary-layer decoupling over cold surfaces as a physical
759 boundary-instability. *Boundary-Layer Meteorology*, 90(2), 297-325.
- 760 Dong, H., Zhang, Y., Tao, T., Du, X., Zou, Y. and Cao, S., 2025. Sensitivity of near-ground
761 wind to PBL schemes, reanalysis data, and nudging in month-long WRF simulations in
762 the Tibetan Plateau with highly complex terrain. *Atmospheric Research*, 323, p.108161.
- 763 Duynkerke, P.G., 1991: Radiation fog: A comparison of model simulation with detailed
764 observations. *Monthly Weather Review*, 119(2), 324-341, [https://doi.org/10.1175/1520-0493\(1991\)119<0324:RFACOM>2.0.CO;2](https://doi.org/10.1175/1520-0493(1991)119<0324:RFACOM>2.0.CO;2).
- 765
- 766 England, D.E. and McNider, R.T., 1995: Stability functions based upon shear functions.
767 *Boundary-Layer Meteorology*, 74(1-2), 113-130.
- 768 Esau, I.N. and Byrkjedal, Ø., 2007: Application of a large-eddy simulation database to
769 optimisation of first-order closures for neutral and stably stratified boundary
770 layers. *Boundary-layer meteorology*, 125(2), 207-225.

- 771 Fernando, H.J.S. and Weil, J.C., 2010: Whither the stable boundary layer? A shift in the
772 research agenda. *Bulletin of the American Meteorological Society*, **91(11)**, 1475-1484.
- 773 Franzke, C.L., Lee, S. and Feldstein, S.B., 2017: Evaluating Arctic warming mechanisms in
774 CMIP5 models. *Climate Dynamics*, **48**, 3247-3260.
- 775 Galperin, B., Sukoriansky, S. and Anderson, P.S., 2007a. On the critical Richardson number
776 in stably stratified turbulence. *Atmospheric Science Letters*, **8(3)**, pp.65-69.
- 777 Galperin, B., Sukoriansky, S. and Perov, V., 2007b: Implementation of the quasi-normal
778 scale elimination (QNSE) turbulence model in WRF. In *The Eighth WRF Users' Workshop*.
779 https://www2.mmm.ucar.edu/wrf/users/workshops/WS2007/presentation/5-6_Galperin.pdf
- 781 Graversen, R.G. and Wang, M., 2009: Polar amplification in a coupled climate model with
782 locked albedo. *Climate Dynamics*, **33**, 629-643.
- 783 Hahn, L.C., Armour, K.C., Zelinka, M.D., Bitz, C.M. and Donohoe, A., 2021. Contributions
784 to polar amplification in CMIP5 and CMIP6 models. *Frontiers in Earth Science*, **9**,
785 p.710036.
- 786 Hall, A., 2004: The role of surface albedo feedback in climate. *Journal of Climate*, **17(7)**,
787 1550-1568.
- 788 Holtslag, A.A.M. and Boville, B.A., 1993: Local versus nonlocal boundary-layer diffusion in
789 a global climate model. *Journal of Climate*, **6(10)**, 1825-1842.
- 790 Janjic ZI. 2001: Nonsingular implementation of the Mellor-Yamada Level 2.5 scheme in the
791 NCEP Meso Model, NOAA/NWS/NCEP Office Note 437.
- 792 Kantha, L.H. and Clayson, C.A., 1994: An improved mixed layer model for geophysical
793 applications. *Journal of Geophysical Research: Oceans*, **99(C12)**, 25235-25266.
- 794 Kosović, B. and Curry, J.A., 2000: A large eddy simulation study of a quasi-steady, stably
795 stratified atmospheric boundary layer. *Journal of the atmospheric sciences*, **57(8)**, 1052-
796 1068
- 797 Louis, J.F., 1979: A parametric model of vertical eddy fluxes in the atmosphere. *Boundary-
798 Layer Meteorology*, **17(2)**, 187-202.
- 799 Mahrt, L., 1989: Limit cycle mixing. *Journal of Atmospheric Sciences*, **46(8)**, 1061-1075.

- 800 Mahrt, L., 1996: The bulk aerodynamic formulation over heterogeneous surfaces. *Boundary-*
801 *Layer Meteorology*, **78(1)**, 87-119.
- 802 Manabe, S. and Stouffer, R.J., 1994: Multiple-century response of a coupled ocean-
803 atmosphere model to an increase of atmospheric carbon dioxide. *Journal of climate*, **7(1)**,
804 5-23.
- 805 Manabe, S. and Wetherald, R.T., 1975: The effects of doubling the CO₂ concentration on the
806 climate of a general circulation model. *Journal of Atmospheric Sciences*, **32(1)**, 3-15.
- 807 McNider, R.T. and Pielke, R.A., 1981: Diurnal boundary-layer development over sloping
808 terrain. *Journal of Atmospheric Sciences*, **38(10)**, 2198-2212.
- 809 McNider, R.T., England, D.E., Friedman, M.J. and Shi, X., 1995: Predictability of the stable
810 atmospheric boundary layer. *Journal of the Atmospheric Sciences*, **52(10)**, 1602-1614.
- 811 McNider, R.T., Pour-Biazar, A., Doty, K., White, A., Wu, Y., Qin, M., Hu, Y., Odman, T.,
812 Cleary, P., Knipping, E. and Dornblaser, B., 2018: Examination of the physical
813 atmosphere in the Great Lakes region and its potential impact on air quality—Overwater
814 stability and satellite assimilation. *Journal of Applied Meteorology and*
815 *Climatology*, **57(12)**, 2789-2816.
- 816 McNider, R.T., Steeneveld, G.J., Holtslag, A.A.M., Pielke, R.A., Mackaro, S., Pour-Biazar,
817 A., Walters, J., Nair, U. and Christy, J., 2012: Response and sensitivity of the nocturnal
818 boundary layer over land to added longwave radiative forcing. *Journal of Geophysical*
819 *Research: Atmospheres*, **117(D14)**.
- 820 Mellor, G. L., 1973: Analytic prediction of the properties of stratified planetary surface
821 layers. *J. Atmos. Sci.*, **30**, 1061-1069.
- 822 Mellor, G.L. and Yamada, T., 1982: Development of a turbulence closure model for
823 geophysical fluid problems. *Reviews of Geophysics*, **20(4)**, 851-875.
- 824 Nielsen-Englyst, P., Høyer, J.L., Kolbe, W.M., Dybkjær, G., Lavergne, T., Tonboe, R.T.,
825 Skarpalezos, S. and Karagali, I., 2023. A combined sea and sea-ice surface temperature
826 climate dataset of the Arctic, 1982–2021. *Remote Sensing of Environment*, **284**,
827 p.113331.
- 828 Pithan, F. and Mauritsen, T., 2014: Arctic amplification dominated by temperature feedbacks
829 in contemporary climate models. *Nature Geoscience*, **7(3)**, 181.

- 830 Pithan, F., Ackerman, A., Angevine, W.M., Hartung, K., Ickes, L., Kelley, M., Medeiros, B.,
831 Sandu, I., Steeneveld, G.J., Sterk, H.A. and Svensson, G., 2016: Select strengths and
832 biases of models in representing the Arctic winter boundary layer over sea ice: the
833 Larcform 1 single column model intercomparison. *Journal of advances in modeling earth*
834 *systems*, **8(3)**, 1345-1357.
- 835 Pleim, J.E., 2007: A combined local and nonlocal closure model for the atmospheric
836 boundary layer. Part I: Model description and testing. *Journal of Applied Meteorology*
837 and *Climatology*, **46(9)**, 1383-1395.
- 838 Savijärvi, H., 2009: Stable boundary layer: Parametrizations for local and larger scales.
839 *Quarterly Journal of the Royal Meteorological Society*, **135(641)**, 914-921.
- 840 Screen, J.A., Deser, C. and Simmonds, I., 2012: Local and remote controls on observed
841 Arctic warming. *Geophysical Research Letters*, **39(10)**.
- 842 Shir, C.C. and Bornstein, R.D., 1977: Eddy exchange coefficients in numerical models of the
843 planetary boundary layer. *Boundary-Layer Meteorology*, **11(2)**, 171-185.
- 844 Steeneveld, G.J., Mauritzen, T., De Bruijn, E.I.F., Vilà-Guerau de Arellano, J., Svensson, G.
845 and Holtslag, A.A.M., 2008a: Evaluation of limited-area models for the representation of
846 the diurnal cycle and contrasting nights in CASES-99. *Journal of Applied Meteorology*
847 and *Climatology*, **47(3)**, 869-887.
- 848 Steeneveld, G.J., Holtslag, A.A.M., Nappo, C.J., Van de Wiel, B.J.H. and Mahrt, L., 2008b:
849 Exploring the possible role of small-scale terrain drag on stable boundary layers over
850 land. *Journal of applied meteorology and climatology*, **47(10)**, 2518-2530.
- 851 Steeneveld, G.J., Van de Wiel, B.J.H. and Holtslag, A.A.M., 2006: Modeling the evolution of
852 the atmospheric boundary layer coupled to the land surface for three contrasting nights in
853 CASES-99. *Journal of the atmospheric sciences*, **63(3)**, 920-935.
- 854 Stull, R.B., 1988: Mean boundary layer characteristics. In *An introduction to boundary layer*
855 *meteorology* (pp. 1-27). Dordrecht: Springer Netherlands.
- 856 Sukoriansky, S., Galperin, B. and Staroselsky, I., 2005: A quasinormal scale elimination
857 model of turbulent flows with stable stratification. *Physics of fluids*, **17(8)**, 085107.

- 858 Sukoriansky, S., 2008: Implementation of the Quasi-Normal Scale Elimination (QNSE)
859 model of stably stratified turbulence in WRF. Report on WRF-DTC Visit of Semion
860 Sukoriansky, June 2008.
- 861 Swanson, K.L., 2013: Emerging selection bias in large-scale climate change
862 simulations. *Geophysical Research Letters*, **40(12)**, 3184-3188.
- 863 Tastula, E.M., Galperin, B., Dudhia, J., LeMone, M.A., Sukoriansky, S. and Vihma, T.,
864 2015a: Methodical assessment of the differences between the QNSE and MYJ PBL
865 schemes for stable conditions. *Quarterly Journal of the Royal Meteorological
866 Society*, **141(691)**, 2077-2089.
- 867 Tastula, E.M., Galperin, B., Sukoriansky, S., Luhar, A. and Anderson, P., 2015b. The
868 importance of surface layer parameterization in modeling of stable atmospheric boundary
869 layers. *Atmospheric Science Letters*, **16**(1), pp.83-88.
- 870 Taylor, P.C., Cai, M., Hu, A., Meehl, J., Washington, W. and Zhang, G.J., 2013: A
871 decomposition of feedback contributions to polar warming amplification. *Journal of
872 Climate*, **26(18)**, 7023-7043.
- 873 Van de Wiel, B. J. H., A. F. Moene, R.J. Ronda H. A. R. De Bruin, and A. A. M. Holtslag,
874 2002b: Intermittent turbulence and oscillations in the stable boundary layer over land.
875 Part II. A system dynamics approach., *J. Atmos. Sci.*, **59**, 2567-2581.
- 876 Van de Wiel, B. J. H., Moene, A. F., Jonker, H. J. J., Baas, P., Basu, S., Donda, J. M. M., . . .
877 Holtslag, A. A. M., 2012: The minimum wind speed for sustainable turbulence in the
878 nocturnal boundary layer. *Journal of Atmospheric Science*, **69**, 3097–3115,
879 <https://doi.org/10.1175/JASD-12-064.1>.
- 880 van de Wiel, B. J. H., Vignon, E., Baas, P., van Hooijdonk, I. G. S., van der Linden, S. J. A.,
881 van Hooft, J. A., . . . Genthon, C., 2017: Regime transitionin near-surface temperature
882 inversions: A conceptual model. *Journal of Atmospheric Sciences*, **74**, 1057–1073,
883 <https://doi.org/10.1175/JAS-D-16-0180.1>.
- 884 Van de Wiel, B.J.H., Ronda, R.J., Moene, A.F., De Bruin, H.A.R. and Holtslag, A.A.M.,
885 2002: Intermittent turbulence and oscillations in the stable boundary layer over land. Part
886 I: A bulk model. *Journal of the Atmospheric Sciences*, **59(5)**, 942-958.

- 887 Vignon, E., van de Wiel, B.J., van Hooijdonk, I.G., Genton, C., van der Linden, S.J., van
888 Hooft, J.A., Baas, P., Maurel, W., Traullé, O. and Casasanta, G., 2017: Stable boundary-
889 layer regimes at Dome C, Antarctica: observation and analysis. *Quarterly Journal of the*
890 *Royal Meteorological Society*, **143(704)**, 1241-1253.
- 891 Viterbo, P. and Beljaars, A.C., 1995: An improved land surface parameterization scheme in
892 the ECMWF model and its validation. *Journal of climate*, **8(11)**, 2716-2748.
- 893 , P., Beljaars, A., Mahfouf, J.F. and Teixeira, J., 1999: The representation of soil moisture
894 freezing and its impact on the stable boundary layer. *Quarterly Journal of the Royal*
895 *Meteorological Society*, **125(559)**, 2401-2426.
- 896 Walters, J. T., R. T. McNider, X. Shi, and W. B. Norris, 2007: Positive surface temperature
897 feedback in the stable nocturnal boundary layer. *Geophys. Res. Lett.*, **34(12)**,
898 <https://doi.org/10.1029/2007GL029505>.
- 899 Wang, Q., Zeng, B., Chen, G. and Li, Y., 2024. Simulation performance of different
900 planetary boundary layer schemes in WRF V4. 3.1 on wind field over Sichuan Basin
901 within" Gray zone" resolution. *EGUsphere*, 2024, pp.1-25.
- 902 Zilitinkevich, S.S. and Esau, I.N., 2003: The effect of baroclinicity on the equilibrium depth
903 of neutral and stable planetary boundary layers. *Quarterly Journal of the Royal*
904 *Meteorological Society*, **129(595)**, 3339-3356, <https://doi.org/10.1256/qj.02.94>.
- 905
- 906
- 907 **Appendix A**
- 908 We believe that the development of a grid correction, as presented in the initial tests here,
909 shows promise in improving the problem of grid dependence in modeling the SBL and SL.
910 This may provide a path to allow coarse grid models to make improved climate predictions in
911 the Arctic. However, the initial results show that further improvements are needed in making
912 the analytical adjustment perform better. Also, the simple Arctic simulation carried out here
913 with such a limited vertical domain needs to be expanded to more realistic settings where grid
914 spacing in models may be much greater. As a final caveat, we note that the approach
915 presented here only addresses the explicit dependence of R_i on Δz (4). It does not address

916 issues of unresolved structure (Blackadar, 1979) or mesoscale energy (Mahrt 1996; Steeneveld et
917 al 2008b), which may add mixing.

918 We hope to carry out future model experiments to look at specifying better correction
919 functions and more realistic settings. However, because of our team's lack of experience
920 with full climate models, we feel publishing these preliminary results can perhaps allow other
921 investigators to make progress in making the modeling SL in Arctic environments less grid-
922 dependent. We outline some paths for improvement below.

923 *a. Numerical Solutions to Find Correction (f_c)*

924 The analytical solution derived and tested here (8) is appealing due to its framework for
925 providing corrected stability functions, f_s , which are longer-tailed (see Figure 6). Previous
926 investigators have shown that longer-tailed forms are necessary to provide additional mixing
927 in coarser grids (Beljaars and Holtslag 1991; Louis 1979; Savijarvi 2009). While this paper
928 lays out a framework for correction, its assumption of a constant $\frac{\Delta\theta}{\Delta V^2}$, or equivalently Ri , does
929 not generally hold. As one moves to more complex and deeper test cases, a different approach
930 may be required (if finding a variable D as described above is not sufficient). Another approach,
931 would be to carry out an “on-the-fly” numerical solution of the ODE given in (5). Here, an ODE
932 solver could be used to solve for $f_c(Ri, \Delta z)$. Because of the suspected dependence on curvature
933 in $\frac{\Delta\theta}{\Delta V^2}$, the stencil in the ODE solver will have to capture the curvature. The ODE might initially
934 be solved at each time step in the model simulation. However, it might be solved less often, such
935 as for how radiation is not called every time step in some models. The correction function, as
936 calculated numerically, would be used to calculate the corrected stability function $f_s * f_c$. While
937 solving the ODE will add computational cost, it should be far less than running a model at a very
938 high vertical resolution. Similar metrics as described above would be used to test the numerical
939 f_c .

940 *b. Changes in Atmospheric Energy Budgets with Grid Corrections*

941 A key factor in Arctic Amplification is how energy budgets behave in models as GHG
942 energy is added. MCN12 showed energy budgets were sensitive to the stability functions
943 employed. The above tests showed a path for making model profiles more invariant with grid
944 spacings. In Arctic climate change simulations, the real test is how the atmospheric and
945 surface energy budgets change with the grid corrections. McNider et al. 2012, for a mid-
946 latitude case, examined energy budgets as GHG energy was added for different stability

947 functions. The GABLS1 protocol used here does not have a surface model; all surface values
948 are specified. For more realistic Arctic cases, changes in energy budgets could be similarly
949 calculated (as in McNider et al. 2012) as the grid is changed and grid corrections
950 ($f_c(Ri, \Delta z)$) are implemented.

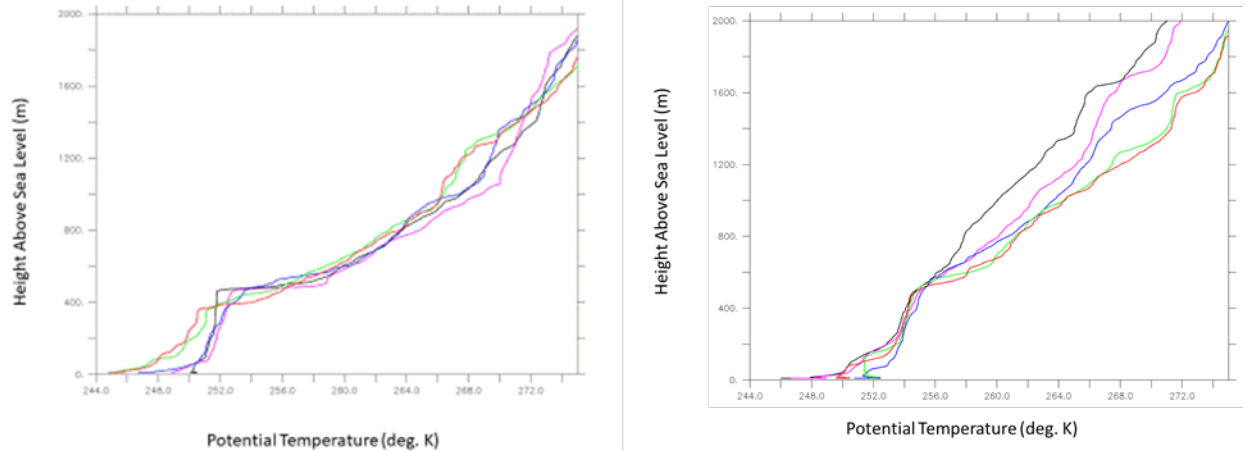
951 *c. Tests of the Corrections Functions in Deeper, More Complex Arctic Profiles*

952 The modeling activities presented here are intended to evaluate and validate the new grid-
953 dependent stability functions discussed above. We focused on the Arctic because of the
954 uncertainty in predicted climate simulations and because of the coarse vertical resolution in
955 climate models, where our approach may be most needed. However, the GABLS1 Arctic case
956 used here is very idealized and shallow, with simple initial conditions (constant temperature
957 profile and barotropic wind profiles).

958 In the GCM and weather forecasting worlds, model domains are much deeper, extending
959 through the troposphere. The limited height domain (400m) of GABLS1 made it impossible
960 for us to look at larger grid spacings beyond 60 m. The GABLS cases have also emphasized
961 near-surface SBL behavior. However, weather forecast models and GCMs must deal with
962 stable layers throughout the troposphere. Figure A1 shows the deep stable layers in Arctic
963 profiles at the Department of Energy ARM Site near Utqiāġvik (previously known as
964 Barrow), Alaska. These deep stable layers are supported by warm air advection aloft by the
965 polar direct cell, which will likely be enhanced by climate change (Cai and Lu 2007). In
966 GCMs at these larger heights, grid spacings may be 200-500 m or larger. Future tests of the
967 grid correction should be conducted in these deeper, more complex settings.

968

969



970

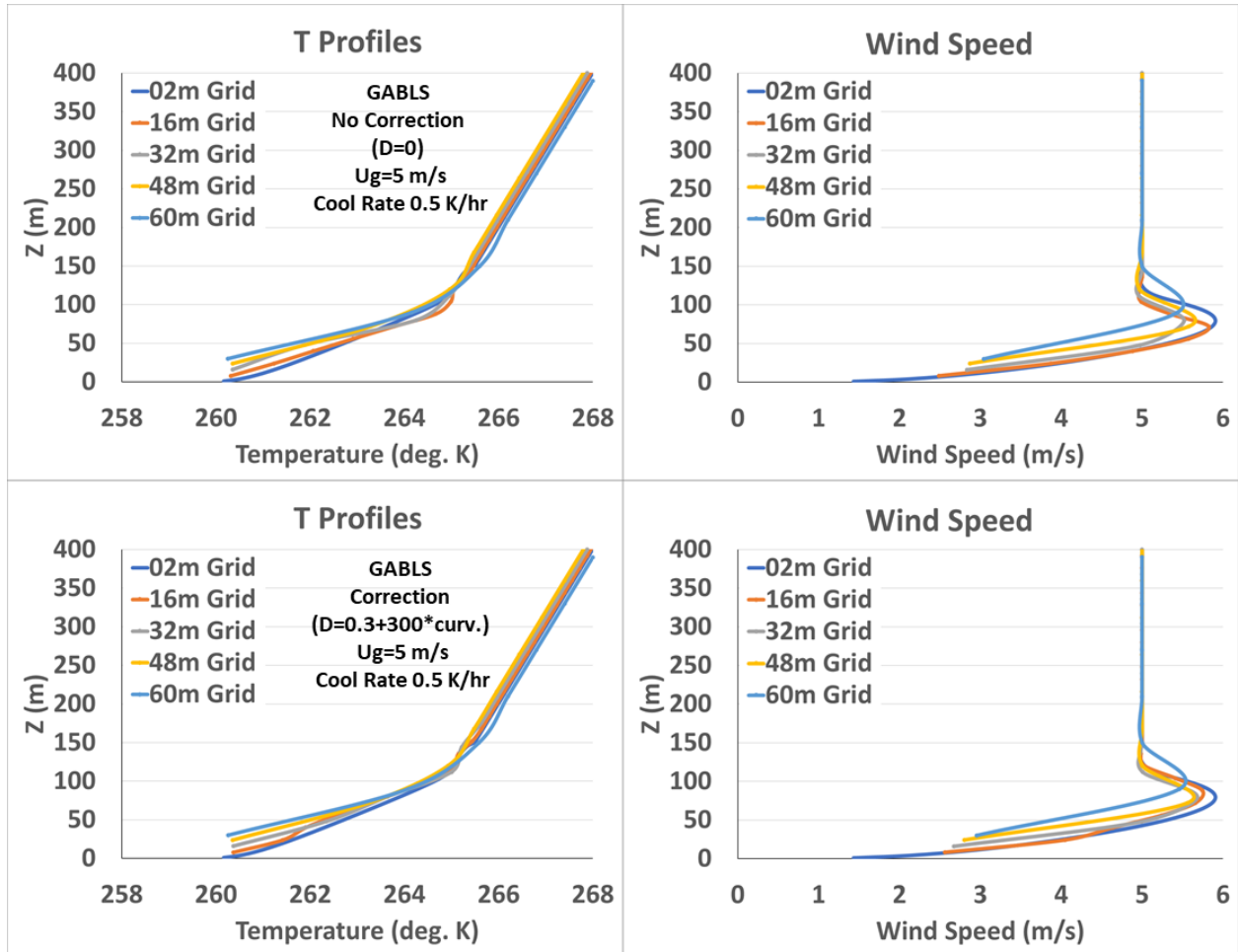
971 Figure A1 Winter potential temperature profiles over ARM's North Slope Alaska site. (left) Dec. 30, 2020,
 972 (right) Jan. 06, 2021. 5:30 (BLACK), 11:00 (PURPLE), 17:30 (BLUE), 21:30 (GREEN), and 23:00
 973 (RED)

974

975

976

977 **Appendix B**

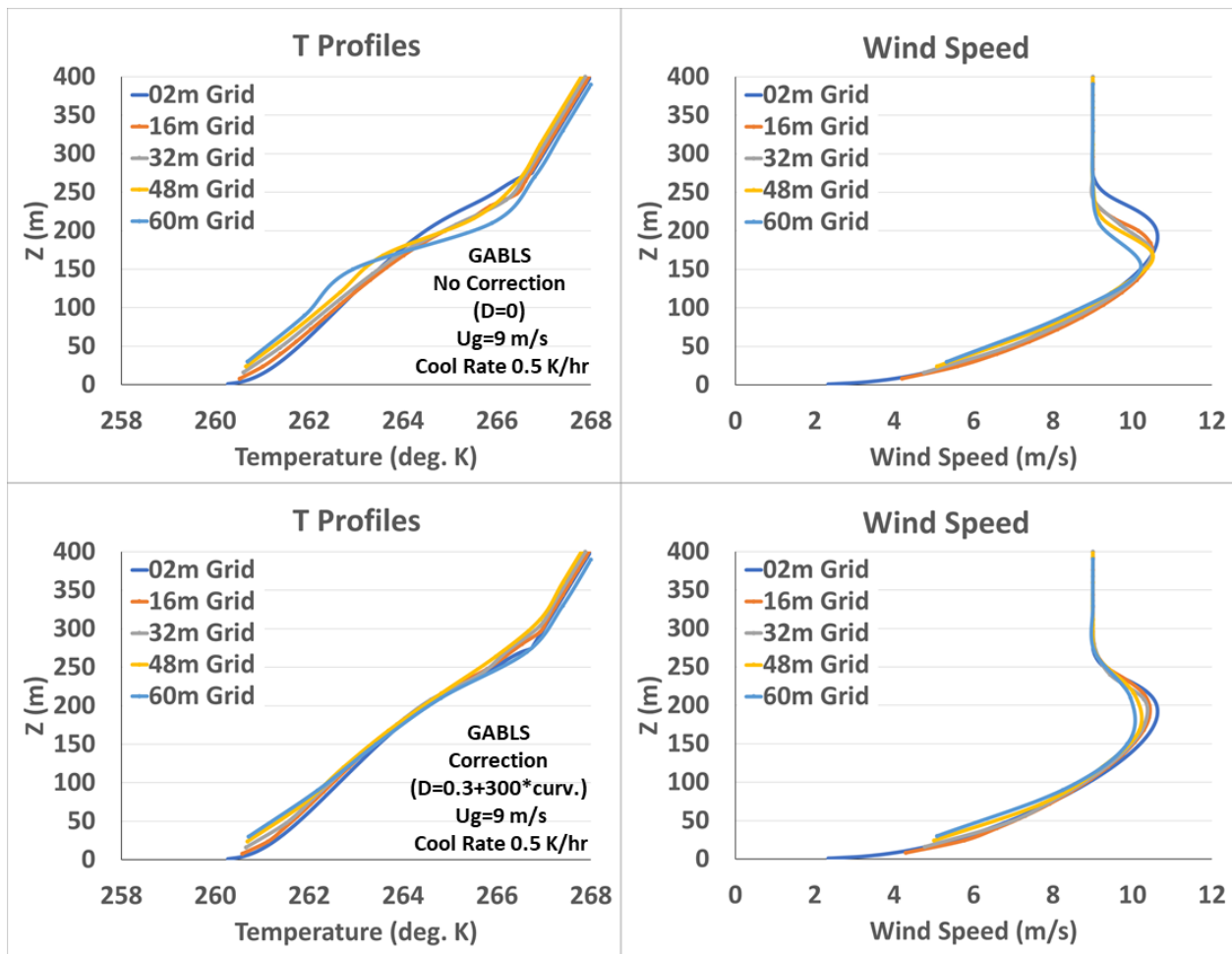


978

979 Figure B1 Plots of temperature and wind speed profiles for geostrophic wind speed of 5
980 m/s and cooling rate of 0.5 K/hr. Top uncorrected and bottom corrected using D in (8)

981

982



983

984 Figure B2 Plots of temperature and wind speed profiles for geostrophic wind speed of 9
 985 m/s and cooling rate of 0.5 K/hr. Top uncorrected and bottom corrected using D in (8)

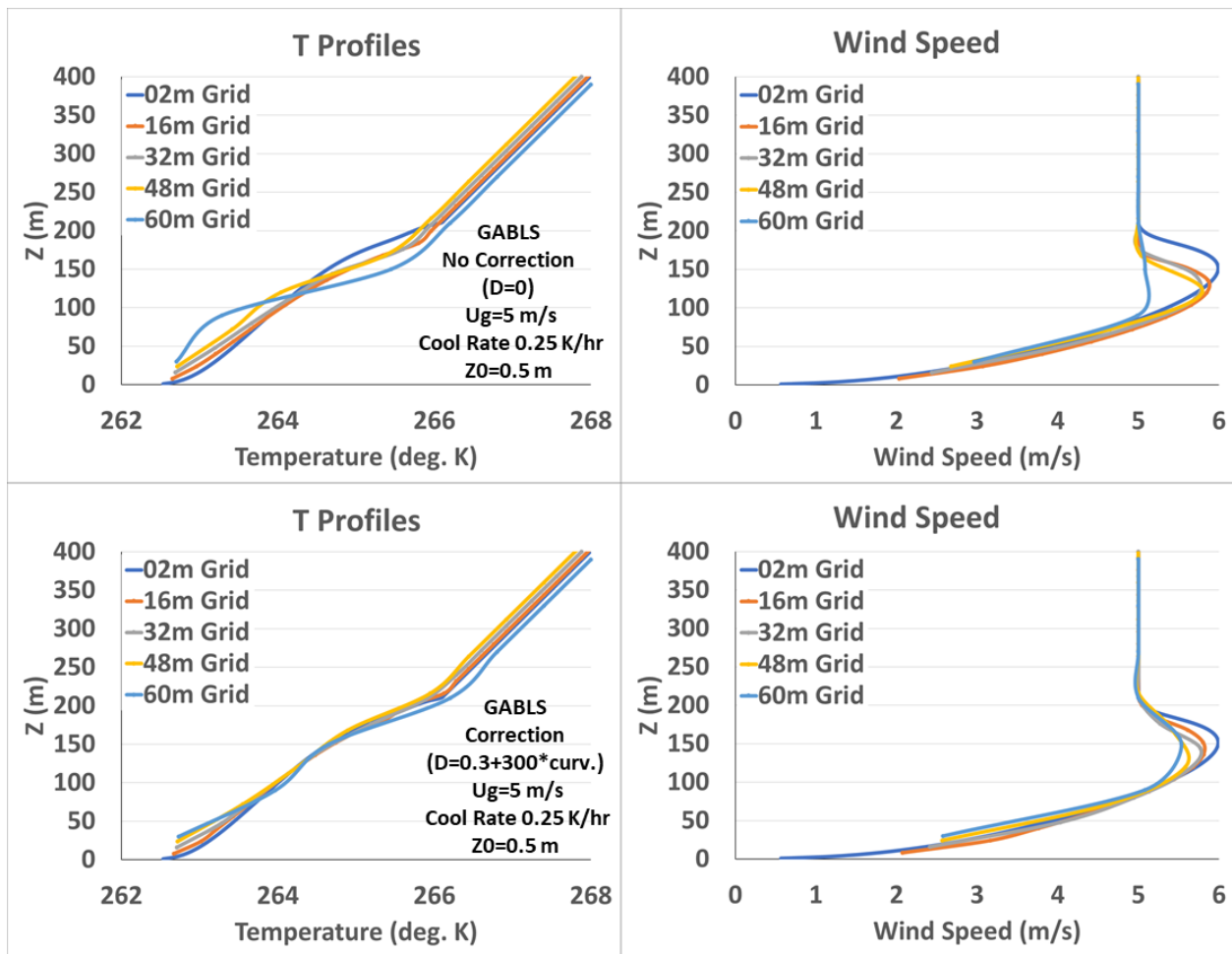
986

987

988

989

990



991

992 **Figure B3** Plots of temperature and wind speed profiles for geostrophic wind speed of 5
 993 m/s cooling rate of 0.25 K/hr and roughness 0.5 m. Top uncorrected and bottom corrected
 994 using D in (8)

995

996

997

998

999

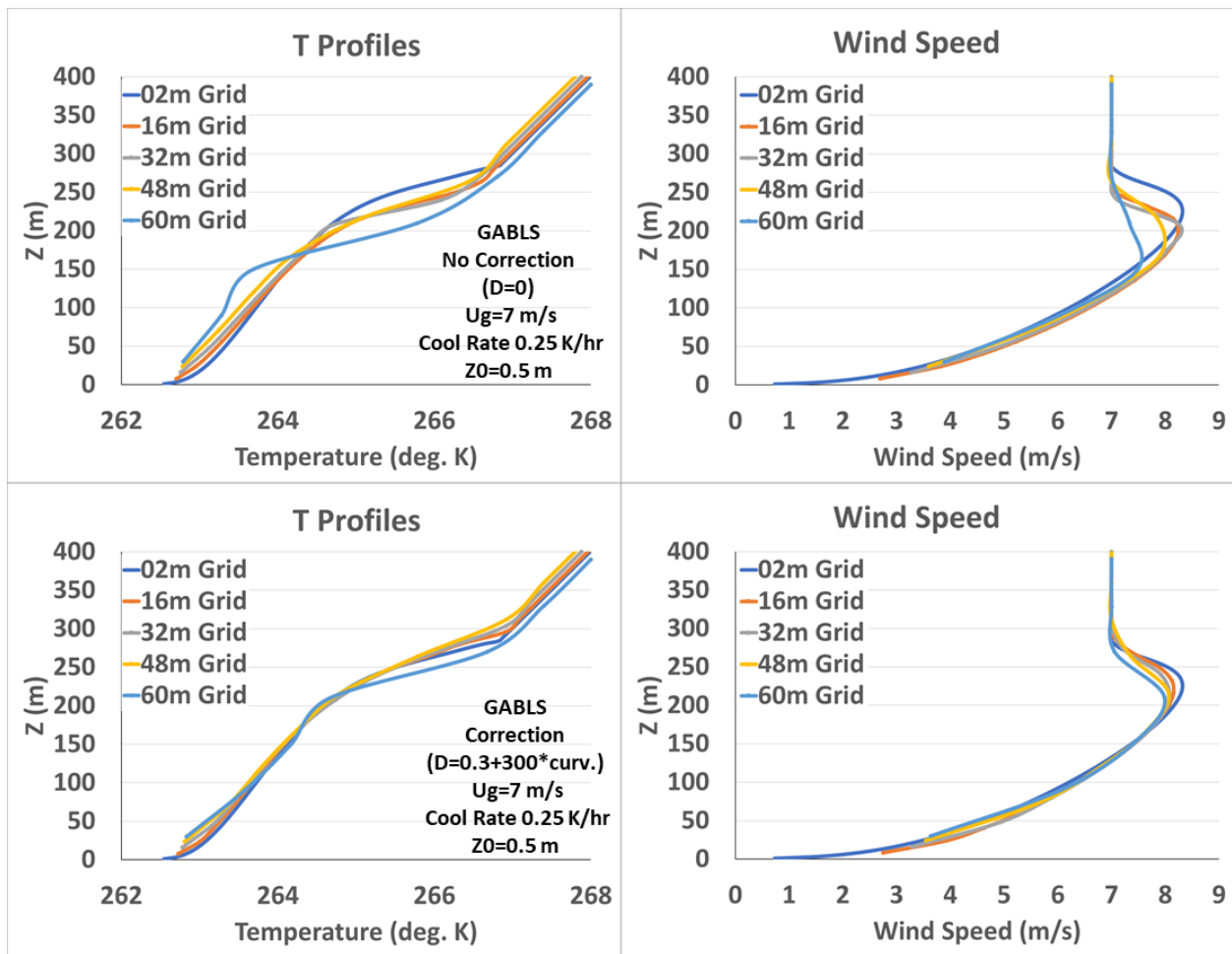


Figure B4 Plots of temperature and wind speed profiles for geostrophic wind speed of 7 m/s cooling rate of 0.25 K/hr and roughness 0.5 m. Top uncorrected and bottom corrected using D in (8)

1004
1005
1006
1007
1008
1009
1010
1011
1012
1013

1014

1015

1016

1017